SPHERICAL DESIGNS FOR APPROXIMATIONS ON SPHERICAL CAPS *

CHAO LI† AND XIAOJUN CHEN‡

Abstract. A spherical t-design is a set of points on the unit sphere, which provides an equal weight quadrature rule integrating exactly all spherical polynomials of degree at most t and has a sharp error bound for approximations on the sphere. This paper introduces a set of points called a spherical cap t-subdesign on a spherical cap $\mathcal{C}(\mathbf{e}_3, r)$ with center $\mathbf{e}_3 = (0, 0, 1)^\top$ and radius $r \in (0, \pi)$ induced by the spherical t-design. We show that the spherical cap t-subdesign provides an equal weight quadrature rule integrating exactly all zonal polynomials of degree at most t and all functions expanded by orthonormal functions on the spherical cap which are defined by shifted Legendre polynomials of degree at most t. We apply the spherical cap t-subdesign and the orthonormal basis functions on the spherical cap to non-polynomial approximation of continuous functions on the spherical cap and present theoretical approximation error bounds. We also apply spherical cap t-subdesigns to sparse signal recovery on the upper hemisphere, which is a spherical cap with $r = 0.5\pi$. Our theoretical and numerical results show that spherical cap t-subdesigns can provide good approximation on spherical caps.

Key words. spherical design, sparse approximation, nonsmooth optimization, spherical caps

AMS subject classifications. 90C26, 90C90, 65D32

1. Introduction.

Let $\mathbb{S}^2 := \{\mathbf{y} \in \mathbb{R}^3 : \|\mathbf{y}\| = 1\} \subset \mathbb{R}^3$ denote the unit sphere, where $\|\cdot\|$ is the Euclidean norm, and let $\mathbb{P}_t(\mathbb{S}^2)$ denote the space of spherical polynomials of degree at most t. The concept of a spherical t-design was introduced by Delsarte, Goethals and Seidel [14], which is a set of points $\{\mathbf{y}_1, \ldots, \mathbf{y}_n\} \subset \mathbb{S}^2$ such that the quadrature rule

$$\frac{1}{4\pi}\int_{\mathbb{S}^2} p(\mathbf{y})d\omega(\mathbf{y}) = \frac{1}{n}\sum_{j=1}^{n} p(\mathbf{y}_j)$$

holds for all polynomials $p \in \mathbb{P}_t(\mathbb{S}^2)$ of degree at most t, where $d\omega(\mathbf{y})$ is the surface measure on $\mathbb{S}^2$. Seymour and Zaslavsky [29] showed that spherical t-designs exist for any t if n is sufficiently large, and the authors in [7] established the optimal asymptotic order for the number of points n required for a spherical t-design. Chen, Frommer and Lang [9] showed existence of spherical t-designs on $\mathbb{S}^2$ with $n = (t+1)^2$ for $t \leq 100$ by using interval methods. Computed spherical t-designs on $\mathbb{S}^2$ with specific t are available in [37]. For more discussion on spherical t-designs, see [1, 5, 8, 33, 34, 39] and references therein.

Spherical t-designs have been extensively studied for various applications and showed good performance on numerical approximation on the sphere. In [2], An et al. studied polynomial approximation problems on the sphere using regularized least squares models and showed that spherical t-designs provide good polynomial approx-

---

*August 22, 2024

†School of Mathematics and Statistics, Taiyuan Normal University, Taiyuan, China; CAS AMSS-PolyU Joint Laboratory of Applied Mathematics, The Hong Kong Polytechnic University, Hong Kong, China (lichao.li@polyu.edu.hk). The work of this author is partially supported by National Natural Science Foundation of China (12301404) and NSF of Shanxi Province (2022D201468).

‡Department of Applied Mathematics, The Hong Kong Polytechnic University, Hong Kong, China (xiaojun.chen@polyu.edu.hk). The work of this author is supported by Hong Kong Research Grant Council PolyU153000212 and CAS-Croucher Funding Scheme for AMSS-PolyU Joint Laboratory. Corresponding author.

imation on the sphere. In [11], Chen and Womersley showed that spherical t-designs provided a sharp error bound for sparse approximation in signal processing on the sphere. In [3, 26], spherical t-designs were applied to interpolation and hyperinterpolation for noisy data on the sphere.

In numerous applications, people are interested in image analysis and signal processing on spherical caps, especially the hemisphere, such as medical images (surfaces of brain, eye, skull, scalp). Good approximations are needed on spherical caps (see for example [12, 21, 22]). How to choose a set of points on spherical caps for good numerical approximation on spherical caps is an interesting and timely question. In this paper, we introduce a set of points on a spherical cap induced by the spherical t-design for good approximations on the spherical cap. Since the sphere is rotationally invariant, we present results on the north polar cap $\mathcal{C}(\mathbf{e}_3, r) := \{\mathbf{x} \in \mathbb{S}^2 : \mathbf{x} \cdot \mathbf{e}_3 \geq \cos r\}$, where $\mathbf{e}_3 = (0,0,1)^\top$, radius $r \in (0,\pi)$ and $\mathbf{x} \cdot \mathbf{e}_3 = \mathbf{x}^\top \mathbf{e}_3$. In spherical polar coordinates, $\mathbb{S}^2$ and $\mathcal{C}(\mathbf{e}_3, r)$ are denoted respectively as

$$\begin{aligned}
\mathbb{S}^2 &= \{\mathbf{y} \in \mathbb{R}^3 : \mathbf{y} := (\sin\vartheta\cos\phi, \sin\vartheta\sin\phi, \cos\vartheta)^\top,\ \vartheta \in [0,\pi],\ \phi \in [0,2\pi]\},\\
\mathcal{C}(\mathbf{e}_3, r) &= \{\mathbf{x} \in \mathbb{R}^3 : \mathbf{x} := (\sin\theta\cos\phi, \sin\theta\sin\phi, \cos\theta)^\top,\ \theta \in [0,r],\ \phi \in [0,2\pi]\}.
\end{aligned}$$

It is easy to verify that for any $\vartheta \in [0,\pi]$, $\arccos(0.5(1-\cos r)(\cos\vartheta - 1) + 1) \in [0, r]$. Now, we introduce the definition of a spherical cap t-subdesign.

Definition 1.1. *Let $\mathcal{C}(\mathbf{e}_3, r)$ be the spherical cap with radius $r \in (0,\pi)$, $\mathcal{Y}_n := \{\mathbf{y}_j \in \mathbb{S}^2 : \mathbf{y}_j = (\sin\vartheta_j\cos\phi_j, \sin\vartheta_j\sin\phi_j, \cos\vartheta_j)^\top,\ \ j = 1,\dots,n\}$ be a spherical t-design and let $\theta_j = \arccos(0.5(1-\cos r)(\cos\vartheta_j - 1) + 1)$, $j = 1,\dots,n$. We call the point set $\mathcal{X}_n^{\mathcal{Y}} := \{\mathbf{x}_j \in \mathcal{C}(\mathbf{e}_3, r) : \mathbf{x}_j = (\sin\theta_j\cos\phi_j, \sin\theta_j\sin\phi_j, \cos\theta_j)^\top, j = 1,\dots,n\}$ a spherical cap t-subdesign induced by the spherical t-design $\mathcal{Y}_n$.*

For convenience, we denote the upper hemisphere (that is $\mathcal{C}(\mathbf{e}_3, 0.5\pi)$) by $\mathbb{S}^2_+$, and call the spherical cap t-subdesign over $\mathbb{S}^2_+$ a hemispherical t-subdesign.

Let $\{Y_{\ell,k} : \ell = 0,1,\dots,t, k = 1,\dots,2\ell+1\}$ be a set of real spherical harmonics orthonormal with respect to the $\mathbb{L}_2$ inner product on $\mathbb{S}^2$, where $Y_{\ell,k}$ is a spherical harmonic of degree ℓ (see for example [4, 13]). It is known [2] that for every $p \in \mathbb{P}_t(\mathbb{S}^2)$, there is a unique vector $\alpha = (\alpha_{\ell,k}) \in \mathbb{R}^{(t+1)^2}$ such that

$$p(\mathbf{x}) = \sum_{\ell=0}^{t}\sum_{k=1}^{2\ell+1} \alpha_{\ell,k} Y_{\ell,k}(\mathbf{x}), \quad \mathbf{x} \in \mathbb{S}^2. \tag{1.1}$$

We call $p = \sum_{\ell=0}^{t} \alpha_{\ell,1} Y_{\ell,1} \in \mathbb{P}_t(\mathbb{S}^2)$ a zonal polynomial of degree at most t on $\mathbb{S}^2$ (see for example [13]). In Section 3, we show that a spherical cap t-subdesign $\mathcal{X}_n^{\mathcal{Y}}$ over $\mathcal{C}(\mathbf{e}_3, r)$ induced by the spherical t-design $\mathcal{Y}_n$ provides equal weight quadrature rules for zonal polynomials, that is,

$$\frac{1}{2\pi(1-\cos r)} \int_{\mathcal{C}(\mathbf{e}_3, r)} p(\mathbf{x}) d\omega(\mathbf{x}) = \frac{1}{n}\sum_{j=1}^{n} p(\mathbf{x}_j), \quad \mathbf{x}_j \in \mathcal{X}_n^{\mathcal{Y}} \tag{1.2}$$

holds for any zonal polynomial $p \in \mathbb{P}_t(\mathbb{S}^2)$.

In [18], the authors introduced a set of hemispherical orthonormal functions $\{H_{\ell,k} : \ell = 0,1,\dots,t, k = 1,\dots,2\ell+1\}$ which are derived from the shifted Legendre polynomials of degree at most t. The set of functions $\{H_{\ell,k}\}$ shows a promising perspective in hemisphere related issues, such as surface description or construction of hemisphere-like anatomical surface [19, 23], rendering and global illumination [18, 25].

Inspired by [18], we define a set of orthonormal functions $\{T^r_{\ell,k}\}$ over a spherical cap $\mathcal{C}(\mathbf{e}_3, r)$ with radius $r \in (0, \pi)$. $\{T^r_{\ell,k}\}$ coincide with $\{H_{\ell,k}\}$ when $r = 0.5\pi$. In Section 3, we show that the spherical cap t-subdesign $\mathcal{X}_n^{\mathcal{Y}}$ provides an equal weight quadrature rule integrating exactly all functions expanded by $\{T^r_{\ell,k}\}$ defined by the shifted Legendre polynomials of degree at most t.

In Section 4, we study the non-polynomial approximation of continuous functions and sparse signal recovery on spherical caps using spherical cap t-subdesigns induced by spherical t-designs and orthonormal functions $\{T^r_{\ell,k}\}$. We derive error bounds in $\mathbb{L}_2$ norm and $\|\cdot\|_\infty$ norm for the non-polynomial approximation, and formulate a non-convex minimization model for sparse signal recovery.

The main contributions of this paper are summarized as follows.

- We define the spherical cap t-subdesign $\mathcal{X}_n^{\mathcal{Y}}$ over $\mathcal{C}(\mathbf{e}_3, r)$ induced by the spherical t-design $\mathcal{Y}_n$, and show that $\mathcal{X}_n^{\mathcal{Y}}$ provides an equal weight quadrature rule for zonal polynomials of degree at most t and all functions expanded by orthonormal functions $\{T^r_{\ell,k}\}$ over $\mathcal{C}(\mathbf{e}_3, r)$ defined by shifted Legendre polynomials of degree at most t. Moreover, we present an addition theorem for $\{T^r_{\ell,k}\}$.
- We derive error bounds of the non-polynomial approximation of continuous functions and present an efficient sparse signal recovery method on $\mathcal{C}(\mathbf{e}_3, r)$ using the spherical cap t-subdesign $\mathcal{X}_n^{\mathcal{Y}}$ and orthonormal functions $\{T^r_{\ell,k}\}$.

The rest of this paper is organized as follows. In Section 2, we give notations, the relationship among $\{Y_{\ell,k}\}$, $\{H_{\ell,k}\}$ and $\{T^r_{\ell,k}\}$, an addition theorem for $\{T^r_{\ell,k}\}$, and an analogues of the Funk-Hecke formula on $\mathcal{C}(\mathbf{e}_3, r)$. In Section 3, we show that the spherical cap t-subdesign $\mathcal{X}_n^{\mathcal{Y}}$ induced by the spherical t-design provides good quadrature rules for a class of functions. In Section 4, we first study the non-polynomial approximation and sparse signal recovery on spherical caps using $\mathcal{X}_n^{\mathcal{Y}}$ and $\{T^r_{\ell,k}\}$. In Section 5, we present numerical evidence on the quality of spherical cap t-subdesigns $\mathcal{X}_n^{\mathcal{Y}}$ for numerical integration, non-polynomial approximation and sparse signal recovery. Finally, we give concluding remarks in Section 6.

2. Notation and preliminaries.

2.1. Notation. Let $\mathbb{N}_0 := \{0, 1, 2, \ldots\}$ denote the set of natural numbers including zero. The geodesic distance on the sphere is $\mathrm{dist}(\mathbf{x}, \mathbf{y}) := \arccos(\mathbf{x} \cdot \mathbf{y})$, for $\mathbf{x}$, $\mathbf{y} \in \mathbb{S}^2$, where $\mathbf{x} \cdot \mathbf{y} = \mathbf{x}^\top \mathbf{y}$ is the inner product of $\mathbf{x}$ and $\mathbf{y}$. We denote a spherical cap with center $\mathbf{y} \in \mathbb{S}^2$ and radius r by $\mathcal{C}(\mathbf{y}, r) := \{\mathbf{x} \in \mathbb{S}^2 : \mathbf{x} \cdot \mathbf{y} \geq \cos r\}$, and the rotation group $\mathrm{SO}(3) := \{\mathbf{R} \in \mathbb{R}^{3\times 3} : \mathbf{R}^\top \mathbf{R} = \mathbf{I}, \det \mathbf{R} = 1\}$, where $\mathbf{I} \in \mathbb{R}^{3\times 3}$ is the identity matrix. We use $\lfloor \cdot \rfloor$ to denote the floor function.

We denote by $\mathbb{L}_2(\Omega)$ the space of square-integrable functions on a nonempty set $\Omega \subseteq \mathbb{S}^2$ endowed with the inner product

$$\langle f, g \rangle_{\mathbb{L}_2(\Omega)} = \int_{\mathbb{S}^2} f(\mathbf{y}) g(\mathbf{y}) d\omega(\mathbf{y}), \quad \forall f, g \in \mathbb{L}_2(\Omega),$$

and the $\mathbb{L}_2$ norm $\|f\|_{\mathbb{L}_2(\Omega)} = (\langle f, f \rangle_{\mathbb{L}_2(\Omega)})^{1/2}$. We denote the space of continuous functions on Ω by $\mathbb{C}(\Omega)$ and define $\|f\|_\infty := \sup_{\mathbf{x} \in \Omega} |f(\mathbf{x})|$ for $f \in \mathbb{C}(\Omega)$.

Let P_ℓ denote a Legendre polynomial of degree ℓ defined as $P_\ell(x) := \frac{1}{2^\ell \ell!} \frac{d^\ell}{dx^\ell}(x^2 - 1)^\ell$, $\forall x \in [-1, 1]$. Let $s \in (-1, 1)$ and $\tilde{P}_\ell(x) := P_\ell(\frac{2(x-1)}{1-s} + 1)$, $x \in [s, 1]$ be a shifted Legendre polynomial of degree ℓ. The shifted Legendre polynomials are orthonormal on $[s, 1]$, that is, $\int_s^1 \tilde{P}_\ell(x) \tilde{P}_{\ell'}(x) dx = \frac{1-s}{2\ell+1} \delta_{\ell\ell'}$, where $\delta_{\ell\ell'} = 1$ if $\ell = \ell'$ and 0 otherwise.

2.2. Spherical harmonics. The standard basis for spherical harmonics of degree $\ell \in \mathbb{N}_0$ is (see for example [4])

$$
\begin{aligned}
Y_{\ell,1}(\vartheta,\phi) &= N_{\ell,0} P_\ell(\cos\vartheta),\\
Y_{\ell,2m}(\vartheta,\phi) &= N_{\ell,m} P_{\ell,m}(\cos\vartheta)\cos m\phi,\\
Y_{\ell,2m+1}(\vartheta,\phi) &= N_{\ell,m} P_{\ell,m}(\cos\vartheta)\sin m\phi, \quad m = 1,\ldots,\ell,
\end{aligned}
$$

where $\vartheta \in [0,\pi]$, $\phi \in [0,2\pi]$, $N_{\ell,m} = \sqrt{\frac{2\ell+1}{2\pi}\frac{(\ell-m)!}{(\ell+m)!}}$, $N_{\ell,0} = \sqrt{\frac{2\ell+1}{4\pi}}$ and $P_{\ell,m}$ is an associated Legendre function, i.e., $P_{\ell,m}(x) = (-1)^m(1-x^2)^{\frac{m}{2}} P_\ell^{(m)}(x)$, $\forall x \in [-1,1]$, $m = 1,\ldots,\ell$. For any $\ell \in \mathbb{N}_0$, $Y_{\ell,1}$ is called a zonal spherical harmonic. For convenience, we denote by $Y_{\ell,k}$ a real-valued spherical harmonic of degree $\ell \in \mathbb{N}_0$, order $k \in \{1,\ldots,2\ell+1\}$ and write $Y_{\ell,k}(\mathbf{y}) := Y_{\ell,k}(\vartheta,\phi)$ with $\mathbf{y} = (\sin\vartheta\cos\phi, \sin\vartheta\sin\phi, \cos\vartheta)^\top \in \mathbb{S}^2$.

The spherical harmonics are $\mathbb{L}_2(\mathbb{S}^2)$-orthonormal to each other, that is,

$$
\int_{\mathbb{S}^2} Y_{\ell,k}(\mathbf{y}) Y_{\ell',k'}(\mathbf{y}) d\omega(\mathbf{y}) = \delta_{\ell\ell'}\delta_{kk'}. \tag{2.1}
$$

The set of spherical harmonics $\{Y_{\ell,k} : k = 1,2,\ldots,2\ell+1,\ \ell = 0,1,\ldots,t\}$ forms a complete $\mathbb{L}_2(\mathbb{S}^2)$-orthonormal basis of $\mathbb{P}_t(\mathbb{S}^2)$. Moreover, $\mathbb{P}_t(\mathbb{S}^2_+) = \operatorname{span}\{Y_{\ell,k}|_{\mathbb{S}^2_+} : k = 1,2,\ldots,2\ell+1,\ \ell = 0,1,\ldots,t\}$, due to the linear independence of $Y_{\ell,k}|_{\mathbb{S}^2_+}$ which are the restrictions of $Y_{\ell,k}$ to the hemisphere. The addition theorem (see for example [4]) for spherical harmonics is

$$
\textstyle\sum_{k=1}^{2\ell+1} Y_{\ell,k}(\mathbf{y}) Y_{\ell,k}(\mathbf{z}) = \frac{2\ell+1}{4\pi} P_\ell(\mathbf{y}\cdot\mathbf{z}), \quad \forall \mathbf{y},\mathbf{z} \in \mathbb{S}^2,\ \forall \ell \in \mathbb{N}_0. \tag{2.2}
$$

We denote

$$
G_t(\mathbf{y},\mathbf{z}) := \textstyle\sum_{\ell=0}^{t}\sum_{k=1}^{2\ell+1} Y_{\ell,k}(\mathbf{y}) Y_{\ell,k}(\mathbf{z}) = \sum_{\ell=0}^{t} \frac{2\ell+1}{4\pi} P_\ell(\mathbf{y}\cdot\mathbf{z}), \quad \forall \mathbf{y},\mathbf{z} \in \mathbb{S}^2, \tag{2.3}
$$

which is a "reproducing kernel" in $\mathbb{P}_t(\mathbb{S}^2)$ [28] and whose value depends only on the inner product $\mathbf{y}\cdot\mathbf{z}$. Obviously, G_t is rotationally invariant, that is, for $\mathbf{y},\mathbf{z} \in \mathbb{S}^2$ and any rotation $\mathbf{R} \in \mathrm{SO}(3)$, $G_t(\mathbf{y},\mathbf{z}) = G_t(\mathbf{R}\mathbf{y},\mathbf{R}\mathbf{z})$.

The Funk-Hecke formula (see for example [13, 16, 17, 20, 27]) which plays an important role in the theory of spherical harmonics gives the following.

LEMMA 2.1 (Funk-Hecke Formula). *Let f be a continuous function on $[-1,1]$, then for any $\ell \in \mathbb{N}_0$,*

$$
\int_{\mathbb{S}^2} f(\mathbf{x}\cdot\mathbf{y}) Y_{\ell,k}(\mathbf{x}) d\omega(\mathbf{x}) = \lambda_\ell Y_{\ell,k}(\mathbf{y}), \quad \forall \mathbf{y} \in \mathbb{S}^2,
$$

where $\lambda_\ell = 2\pi\int_{-1}^{1} f(t)P_\ell(t)dt$.

Based on the Funk-Hecke formula and Slepian functions [30] on a spherical cap $\mathcal{C}(\mathbf{e}_3, r)$ (see Appendix A for more detail), we obtain the following proposition.

PROPOSITION 2.2. *Let f be a continuous function on $[-1,1]$. For any $L \in \mathbb{N}_0$ and any $\mathbf{y} \in \mathbb{S}^2$, let $\mathbf{Y}_L^\lambda(\mathbf{y}) = (\lambda_0 Y_{0,1}(\mathbf{y}), \lambda_1 Y_{1,1}(\mathbf{y}), \lambda_1 Y_{1,2}(\mathbf{y}), \ldots, \lambda_L Y_{L,2L+1}(\mathbf{y}))^\top$, where $\lambda_j = 2\pi\int_{-1}^{1} f(t)P_j(t)dt$, $j = 0,1,\ldots,L$. For any fixed $r \in (0,\pi)$ and $\ell \le L$, we have*

$$
\int_{\mathcal{C}(\mathbf{e}_3,r)} f(\mathbf{x}\cdot\mathbf{y}) Y_{\ell,k}(\mathbf{x}) d\omega(\mathbf{x}) = \mathbf{c}_{\ell,k}\mathbf{Y}_L^\lambda(\mathbf{y}), \quad \forall \mathbf{y} \in \mathbb{S}^2, \tag{2.4}
$$

where $\mathbf{c}_{\ell,k} := \mathbf{v}_{\ell,k}\mathbf{\Lambda}\mathbf{V}^\top$*,* $\mathbf{\Lambda} = \mathrm{diag}(\rho_1, \ldots, \rho_{L,2L+1})$ *and* $\mathbf{V} = (\mathbf{v}_1, \ldots, \mathbf{v}_{L,2L+1})$ *with* $\rho_i, \mathbf{v}_i$ *being the ith largest eigenvalue and corresponding eigenvector of the matrix* $\mathbf{D}$ *defined by (A.1) with* $t = L$*, and* $\mathbf{v}_{\ell,k}$ *is the* $(\ell^2 + k)$*th row of the matrix* $\mathbf{V}$*.*

Proof. First we assume that f is a polynomial of degree $L \in \mathbb{N}_0$ and let $d_L := (L+1)^2$. By Appendix A, the Slepian functions of degree $\le L$ over $\mathcal{C}(\mathbf{e}_3, r)$ are $S_i(\mathbf{x}) = \sum_{j=0}^{L}\sum_{k=1}^{2j+1} v_{j,k}^i Y_{j,k}(\mathbf{x})$, $\forall \mathbf{x} \in \mathcal{C}(\mathbf{e}_3, r)$, $i = 1, \ldots, d_L$. And, $Y_{\ell,k}(\mathbf{x}) = \sum_{i=1}^{d_L} v_{\ell,k}^i S_i(\mathbf{x})$, $\forall \mathbf{x} \in \mathbb{S}^2$, $k \in \{1, \ldots, 2\ell + 1\}$, $\ell \le L$. Then, for any $\ell \le L$, we have

$$\begin{aligned}
&\textstyle\int_{\mathcal{C}(\mathbf{e}_3,r)} f(\mathbf{x}\cdot\mathbf{y})Y_{\ell,k}(\mathbf{x})d\omega(\mathbf{x})\\
&= \textstyle\sum_{i=1}^{d_L} v_{\ell,k}^i \int_{\mathcal{C}(\mathbf{e}_3,r)} f(\mathbf{x}\cdot\mathbf{y})S_i(\mathbf{x})d\omega(\mathbf{x}) = \sum_{i=1}^{d_L} v_{\ell,k}^i \rho_i \int_{\mathbb{S}^2} f(\mathbf{x}\cdot\mathbf{y})S_i(\mathbf{x})d\omega(\mathbf{x})\\
&= \textstyle\sum_{i=1}^{d_L} v_{\ell,k}^i \rho_i \sum_{j=0}^{L}\sum_{k'=1}^{2j+1} v_{j,k'}^i \int_{\mathbb{S}^2} f(\mathbf{x}\cdot\mathbf{y})Y_{j,k'}(\mathbf{x})d\omega(\mathbf{x})\\
&= \textstyle\sum_{i=1}^{d_L} v_{\ell,k}^i \rho_i \sum_{j=0}^{L}\sum_{k'=1}^{2j+1} v_{j,k'}^i \lambda_j Y_{j,k'}(\mathbf{y}) = \mathbf{c}_{\ell,k}\mathbf{Y}_L^\lambda(\mathbf{y}), \quad \forall \mathbf{y} \in \mathbb{S}^2,
\end{aligned}$$

where the first and third equalities follow from the relationship between S_i and $Y_{\ell,k}$, the second equality follows from (A.3) and, for any fixed $\mathbf{y} \in \mathbb{S}^2$, $f(\mathbf{x}\cdot\mathbf{y})$ is a spherical polynomial of degree $\le L$, and the last equality follows from the Funk-Hecke formula.

Now, if f is a continuous function on $[-1, 1]$, then we choose a sequence of polynomials p_L of degree L such that p_L converges to f uniformly on $[-1, 1]$. It follows that for L sufficiently large, the desired result holds for f. The proof is completed. □

Remark 2.3. Notice that the matrix $\mathbf{D}$ defined by (A.1) is an identity matrix when $r = \pi$, $t = L$. Then, $\rho_i = 1$ and $\mathbf{v}_i$ is a unit vector with the ith element being 1. Thus, (2.4) reduces to the Funk-Hecke Formula.

2.3. Orthogonal functions on spherical caps. In [18], Gautron et al. propose a set of real-valued hemispherical orthogonal functions derived from a shifted Legendre polynomial of degree $\ell \in \mathbb{N}_0$, which have the following form

$$\begin{aligned}
H_{\ell,1}(\theta,\phi) &= \sqrt{2}N_{\ell,0}\tilde{P}_\ell(\cos\theta),\\
H_{\ell,2m}(\theta,\phi) &= \sqrt{2}N_{\ell,m}\tilde{P}_{\ell,m}(\cos\theta)\cos m\phi,\\
H_{\ell,2m+1}(\theta,\phi) &= \sqrt{2}N_{\ell,m}\tilde{P}_{\ell,m}(\cos\theta)\sin m\phi, \quad m = 1, 2, \ldots, \ell,
\end{aligned}$$

where $\theta \in [0, \frac{\pi}{2}]$, $\phi \in [0, 2\pi]$, $\tilde{P}_{\ell,m}(\cos\theta) := P_{\ell,m}(2\cos\theta - 1)$. For convenience, we write $H_{\ell,k}(\mathbf{x}) := H_{\ell,k}(\theta,\phi)$, $k \in \{1, \ldots, 2\ell+1\}$ with $\mathbf{x} = (\sin\theta\cos\phi, \sin\theta\sin\phi, \cos\theta)^\top \in \mathbb{S}^2_+$.

Remark 2.4. Although $\{H_{\ell,k}\}$ are called hemispherical harmonics in [19, 23, 25], $\{H_{\ell,k}\}$ are not harmonic functions on $\mathbb{S}^2_+$. For example, for $\ell = 1$ and $k = 2$,

$$\begin{aligned}
H_{1,2}(\mathbf{x}) = H_{1,2}(\theta,\phi) &= 2\sqrt{\tfrac{3}{8\pi}}\tilde{P}_{1,1}(\cos\theta)\cos\phi\\
&= \sqrt{\tfrac{3}{2\pi}}(-1)^1(1 - (2\cos\theta - 1)^2)^{\frac{1}{2}}\cos\phi = -x\sqrt{\tfrac{6}{\pi}}\sqrt{\tfrac{z}{1+z}},
\end{aligned}$$

where $\mathbf{x} = (x, y, z)^\top = (\sin\theta\cos\phi, \sin\theta\sin\phi, \cos\theta)^\top \in \mathbb{S}^2_+$. Thus,

$$\nabla^2 H_{1,2}(\mathbf{x}) = \frac{\partial^2 H_{1,2}(\mathbf{x})}{\partial x^2} + \frac{\partial^2 H_{1,2}(\mathbf{x})}{\partial y^2} + \frac{\partial^2 H_{1,2}(\mathbf{x})}{\partial z^2} = \frac{\partial^2 H_{1,2}(\mathbf{x})}{\partial z^2} \ne 0,$$

which implies that $H_{1,2}$ is not a harmonic function.

Similarly, we define a set of orthonormal functions over a spherical cap $\mathcal{C}(\mathbf{e}_3, r)$ with $r \in (0, \pi)$ derived from a shifted Legendre polynomial of degree $\ell \in \mathbb{N}_0$ as follows,

$$T_{\ell,1}^r(\theta,\phi) = \sqrt{\kappa}N_{\ell,0}P_\ell(\kappa\cos\theta + 1 - \kappa),$$

$$T^r_{\ell,2m}(\theta,\phi) = \sqrt{\kappa} N_{\ell,m} P_{\ell,m}(\kappa\cos\theta + 1 - \kappa)\cos m\phi,$$
$$T^r_{\ell,2m+1}(\theta,\phi) = \sqrt{\kappa} N_{\ell,m} P_{\ell,m}(\kappa\cos\theta + 1 - \kappa)\sin m\phi, \quad m = 1,2,\ldots,\ell,$$

where $\theta \in [0,r]$, $\phi \in [0,2\pi]$, $\kappa := 2/(1-\cos r)$. For convenience, we write $T^r_{\ell,k}(\mathbf{x}) := T^r_{\ell,k}(\theta,\phi)$, $k \in \{1,2,\ldots,2\ell+1\}$ with $\mathbf{x} = (\sin\theta\cos\phi, \sin\theta\sin\phi, \cos\theta)^\top \in \mathcal{C}(\mathbf{e}_3, r)$.

Notice that $H_{\ell,k} = T^{0.5\pi}_{\ell,k}$, $\forall \ell \in \mathbb{N}_0$, $k = 1,\ldots,2\ell+1$. The functions $\{T^r_{\ell,k}\}$ are $\mathbb{L}_2(\mathcal{C}(\mathbf{e}_3,r))$-orthonormal to each other, i.e.,

$$\int_{\mathcal{C}(\mathbf{e}_3,r)} T^r_{\ell,k}(\mathbf{x}) T^r_{\ell',k'}(\mathbf{x}) d\omega(\mathbf{x}) = \delta_{\ell\ell'}\delta_{kk'}. \tag{2.5}$$

Following the definitions of $\{T^r_{\ell,k}\}$ and $\{Y_{\ell,k}\}$, we have the following proposition.

Proposition 2.5. *Let $r \in (0,\pi)$ be fixed and $\kappa := 2/(1-\cos r)$. For any $\theta \in [0,r]$, let $\vartheta = \arccos(\kappa\cos\theta + 1 - \kappa)$. Then, $\vartheta \in [0,\pi]$ and*

$$T^r_{\ell,k}(\theta,\phi) = \sqrt{\kappa} Y_{\ell,k}(\vartheta,\phi), \quad \forall \ell \in \mathbb{N}_0,\ k \in \{1,2,\ldots,2\ell+1\}. \tag{2.6}$$

In particular, $H_{\ell,k}(\theta,\phi) = \sqrt{2} Y_{\ell,k}(\vartheta,\phi)$.

Now we give the relation between $\{Y_{\ell,k}\}$ and $\{T^r_{\ell,k}\}$ at $\mathbf{x} \in \mathcal{C}(\mathbf{e}_3,r)$.

Proposition 2.6. *Let $r \in (0,\pi)$ be fixed and $\kappa := 2/(1-\cos r)$. For $\ell \in \mathbb{N}_0$ and $k \in \{1,2,\ldots,2\ell+1\}$, let $\nu = \lfloor k/2 \rfloor$ and $\beta_j = \sqrt{\kappa} a_j N_{\ell,\nu}/N_{j,\nu}$ if $\nu \neq 0$, otherwise, $\beta_j = a_j N_{\ell,0}/(\sqrt{\kappa} N_{j,0})$, where $a_j = 0.5\kappa(2j+1)\int_{\cos r}^1 P_\ell(x) P_j(\kappa x + 1 - \kappa) dx$, $j = \nu,\ldots,\ell$, then*

$$\left(\frac{\kappa^2 \mathbf{x}\cdot\mathbf{e}_3 + 2\kappa - \kappa^2}{1 + \mathbf{x}\cdot\mathbf{e}_3}\right)^{\frac{\nu}{2}} Y_{\ell,k}(\mathbf{x}) = \sum_{j=\nu}^{\ell} \beta_j T^r_{j,k}(\mathbf{x}), \quad \forall \mathbf{x} \in \mathcal{C}(\mathbf{e}_3,r). \tag{2.7}$$

In particular, $\left(\frac{4\mathbf{x}\cdot\mathbf{e}_3}{1+\mathbf{x}\cdot\mathbf{e}_3}\right)^{\frac{\nu}{2}} Y_{\ell,k}(\mathbf{x}) = \sum_{j=\nu}^{\ell} \beta_j H_{j,k}(\mathbf{x})$, $\forall \mathbf{x} \in \mathbb{S}^2_+$.

Proof. For any $\ell \in \mathbb{N}_0$, $\theta \in [0,r]$ and $\phi \in [0,2\pi]$, let

$$\psi_{\ell,1}(\theta,\phi) = \sqrt{\kappa} N_{\ell,0} P_\ell(\kappa\cos\theta + 1 - \kappa),$$
$$\psi_{\ell,2m}(\theta,\phi) = (-1)^m \sqrt{\kappa} N_{\ell,m} P^{(m)}_\ell(\kappa\cos\theta + 1 - \kappa)\sin^m\theta\cos m\phi,$$
$$\psi_{\ell,2m+1}(\theta,\phi) = (-1)^m \sqrt{\kappa} N_{\ell,m} P^{(m)}_\ell(\kappa\cos\theta + 1 - \kappa)\sin^m\theta\sin m\phi, \quad m = 1,\ldots,\ell.$$

For convenience, we write $\psi_{\ell,k}(\mathbf{x}) := \psi_{\ell,k}(\theta,\phi)$, $k \in \{1,2,\ldots,2\ell+1\}$, with $\mathbf{x} = (\sin\theta\cos\phi, \sin\theta\sin\phi, \cos\theta)^\top \in \mathcal{C}(\mathbf{e}_3,r)$.

We can see that

$$\begin{aligned} P_{\ell,m}(\kappa\cos\theta + 1 - \kappa) &= (-1)^m (1 - (\kappa\cos\theta + 1 - \kappa)^2)^{\frac{m}{2}} P^{(m)}_\ell(\kappa\cos\theta + 1 - \kappa) \\ &= (-1)^m \left(\tfrac{\kappa^2\cos\theta + 2\kappa - \kappa^2}{1+\cos\theta}\right)^{\frac{m}{2}} P^{(m)}_\ell(\kappa\cos\theta + 1 - \kappa)\sin^m\theta, \end{aligned}$$

which implies

$$T^r_{\ell,k}(\mathbf{x}) = \left(\tfrac{\kappa^2\mathbf{x}\cdot\mathbf{e}_3 + 2\kappa - \kappa^2}{1+\mathbf{x}\cdot\mathbf{e}_3}\right)^{\frac{\nu}{2}} \psi_{\ell,k}(\mathbf{x}),\ \forall \mathbf{x} \in \mathcal{C}(\mathbf{e}_3,r). \tag{2.8}$$

On the other hand, for $\theta \in [0, r]$,

$$\begin{aligned} N_{\ell,m}P_{\ell,m}(\cos\theta) &= N_{\ell,m}(-1)^m(1-\cos^2\theta)^{\frac{m}{2}}P_\ell^{(m)}(\cos\theta) \\ &= \textstyle\sum_{j=m}^{\ell} \frac{\kappa a_j N_{\ell,m}}{N_{j,m}}(-1)^m N_{j,m}P_j^{(m)}(\kappa\cos\theta+1-\kappa)\sin^m\theta \\ &= \textstyle\sum_{j=m}^{\ell} \beta_j(-1)^m\sqrt{\kappa}N_{j,m}P_j^{(m)}(\kappa\cos\theta+1-\kappa)\sin^m\theta, \\ N_{\ell,0}P_\ell(\cos\theta) &= \textstyle\sum_{j=0}^{\ell} \beta_j\sqrt{\kappa}N_{j,0}P_j(\kappa\cos\theta+1-\kappa), \end{aligned}$$

where the second and last equalities follow from definition of a_j. Thus, by definitions of $\psi_{\ell,k}$ and $Y_{\ell,k}$, we have

$$Y_{\ell,k}(\mathbf{x}) = \textstyle\sum_{j=\nu}^{\ell} \beta_j\psi_{j,k}(\mathbf{x}), \quad \forall \mathbf{x} \in \mathcal{C}(\mathbf{e}_3, r). \tag{2.9}$$

Multiplying $\left(\frac{\kappa^2\mathbf{x}\cdot\mathbf{e}_3+2\kappa-\kappa^2}{1+\mathbf{x}\cdot\mathbf{e}_3}\right)^{\frac{\nu}{2}}$ on both sides of (2.9), combing (2.8), we obtain (2.7). Taking $r = 0.5\pi$, we obtain the rest of the proposition. The proof is completed. ∎

Remark 2.7. Let $s \in (-1, 1)$, $\tilde{P}_\ell(x) := P_\ell(\frac{2(x-1)}{1-s}+1)$, $x \in [s, 1]$. Let $\mathbb{P}_\ell([-1, 1])$ be the space of polynomials of degree at most ℓ on $[-1, 1]$. It is easy to see (see for example [24]) that $\tilde{P}_\ell \in \mathbb{P}_\ell([-1, 1])$. Thus, $\tilde{P}_\ell(x) = \sum_{j=0}^{\ell} b_jP_j(x)$, $x \in [s, 1]$, where $b_j = \frac{2j+1}{2}\int_{-1}^{1}\tilde{P}_\ell(x)P_j(x)dx$. Moreover, $\tilde{P}_\ell^{(m)}(x) = \sum_{j=m}^{\ell} b_jP_j^{(m)}(x)$, $m = 1, \ldots, \ell$, $\forall x \in [s, 1]$. For $\ell \in \mathbb{N}_0$, $k \in \{1, 2, \ldots, 2\ell+1\}$, let $\nu = \lfloor k/2 \rfloor$, $\gamma_j = \sqrt{\kappa}b_jN_{\ell,\nu}/N_{j,\nu}$, $j = \nu, \ldots, \ell$. Following a similar argument of Proposition 2.6, for any $\ell \in \mathbb{N}_0$, $k \in \{1, 2, \ldots, 2\ell+1\}$, we obtain,

$$T_{\ell,k}^r(\mathbf{x}) = \left(\frac{\kappa^2\mathbf{x}\cdot\mathbf{e}_3+2\kappa-\kappa^2}{1+\mathbf{x}\cdot\mathbf{e}_3}\right)^{\frac{\nu}{2}} \textstyle\sum_{j=\nu}^{\ell} \gamma_jY_{j,k}(\mathbf{x}), \quad \forall \mathbf{x} \in \mathcal{C}(\mathbf{e}_3, r), \tag{2.10}$$

which shows that $\{T_{\ell,k}^r\}$ are not polynomials except when $k = 1$.

We next present an addition theorem for $\{T_{\ell,k}^r\}$.

THEOREM 2.8. *Let $\mathcal{C}(\mathbf{e}_3, r)$ be the spherical cap with radius $r \in (0, \pi)$. For any $\ell \in \mathbb{N}_0$ and $\mathbf{x}, \mathbf{z} \in \mathcal{C}(\mathbf{e}_3, r)$, there is a rotation matrix $\mathbf{R}_{\mathbf{xz}} \in \mathrm{SO}(3)$ such that*

$$\sum_{k=1}^{2\ell+1} T_{\ell,k}^r(\mathbf{x})T_{\ell,k}^r(\mathbf{z}) = \frac{2\ell+1}{2\pi(1-\cos r)}P_\ell(\mathbf{x}^\top\mathbf{R}_{\mathbf{xz}}\mathbf{z}). \tag{2.11}$$

In particular, (i) $\sum_{k=1}^{2\ell+1} H_{\ell,k}(\mathbf{x})H_{\ell,k}(\mathbf{z}) = \frac{2\ell+1}{2\pi}P_\ell(\mathbf{x}^\top\mathbf{R}_{\mathbf{xz}}\mathbf{z})$, $\forall \mathbf{x}, \mathbf{z} \in \mathbb{S}_+^2$. (ii) $\mathbf{R}_{\mathbf{xz}} = \mathbf{I}$ when $\mathbf{x} = \mathbf{z}$.

Proof. Let $r \in (0, \pi)$ be fixed and $\kappa := 2/(1-\cos r)$. For any $(\theta, \phi) \in [0, r]\times[0, 2\pi]$, let $\gamma = \arccos(\kappa\cos\theta+1-\kappa) - \theta$ and

$$\mathcal{R}(\theta, \phi) := \begin{bmatrix} \cos^2\phi\cos\gamma+\sin^2\phi & (\cos\gamma-1)\cos\phi\sin\phi & \cos\phi\sin\gamma \\ (\cos\gamma-1)\cos\phi\sin\phi & \sin^2\phi\cos\gamma+\cos^2\phi & \sin\phi\sin\gamma \\ -\cos\phi\sin\gamma & -\sin\phi\sin\gamma & \cos\gamma \end{bmatrix}. \tag{2.12}$$

Let $\mathbf{R}_{\mathbf{xz}} = \mathcal{R}(\theta_1, \phi_1)^\top\mathcal{R}(\theta_2, \phi_2)$, where (θ_1, ϕ_1), $(\theta_2, \phi_2) \in [0, r]\times[0, 2\pi]$ are the polar coordinates of $\mathbf{x}$, $\mathbf{z} \in \mathcal{C}(\mathbf{e}_3, r)$, respectively. It is easy to verify that $\mathcal{R}(\theta_1, \phi_1)$, $\mathcal{R}(\theta_2, \phi_2)$, $\mathbf{R}_{\mathbf{xz}} \in \mathrm{SO}(3)$. Moreover, $\mathbf{Rx} := \mathcal{R}(\theta_1, \phi_1)\mathbf{x} \in \mathbb{S}^2$ and $\mathbf{Rz} := \mathcal{R}(\theta_2, \phi_2)\mathbf{z} \in \mathbb{S}^2$. By Proposition 2.5,

$$\sum_{k=1}^{2\ell+1} T_{\ell,k}^r(\mathbf{x})T_{\ell,k}^r(\mathbf{z}) = \kappa\sum_{k=1}^{2\ell+1} Y_{\ell,k}(\mathbf{Rx})Y_{\ell,k}(\mathbf{Rz}) = \frac{\kappa(2\ell+1)}{4\pi}P_\ell(\mathbf{x}^\top\mathbf{R}_{\mathbf{xz}}\mathbf{z}),$$

where the last equality follows from (2.2). Thus, (2.11) holds. Taking $r = 0.5\pi$, we obtain (i), and (ii) follows from definition of $\mathbf{R}_{\mathbf{xz}}$. The proof is completed. $\square$

Remark 2.9. In [15], the authors provided an addition theorem for $\{H_{\ell,k}\}$ as

$$\tilde{P}_\ell(\mathbf{x}_1 \cdot \mathbf{x}_2) = \frac{2\pi}{2\ell+1} \sum_{k=1}^{2\ell+1} H_{\ell,k}(\mathbf{x}_1) H_{\ell,k}(\mathbf{x}_2), \quad \forall \mathbf{x}_1, \mathbf{x}_2 \in \mathbb{S}^2_+. \tag{2.13}$$

However, the following example shows that the equality in (2.13) does not hold.

Let $\ell = 1$, $\mathbf{x}_1 = (1, 0, 0)^\top$ and $\mathbf{x}_2 = (\sqrt{3}/2, 0, 1/2)^\top$, we have $H_{1,2}(\mathbf{x}_1) = H_{1,3}(\mathbf{x}_1) = 0$, $H_{1,1}(\mathbf{x}_1) = -\sqrt{3/2\pi}$ and $H_{1,1}(\mathbf{x}_2) = H_{1,3}(\mathbf{x}_2) = 0$, $H_{1,2}(\mathbf{x}_2) = \sqrt{3/2\pi}$. Thus, $\frac{2\pi}{3} \sum_{k=1}^{3} H_{1,k}(\mathbf{x}_1) H_{1,k}(\mathbf{x}_2) = 0$, but

$$\tilde{P}_1(\mathbf{x}_1 \cdot \mathbf{x}_2) = \tilde{P}_1(\sqrt{3}/2) = P_1(\sqrt{3} - 1) = \sqrt{3} - 1 \neq 0,$$

which implies that (2.13) in [15] is not correct.

Remark 2.10. Let $\{T^r_{\ell,k}\}$ be the set of orthonormal functions over $\mathcal{C}(\mathbf{e}_3, r)$, let $\mathcal{C}(\bar{\mathbf{x}}, r)$ be another spherical cap with center $\bar{\mathbf{x}} \in \mathbb{S}^2$ and the same radius r, and $\mathbf{R} \in \mathrm{SO}(3)$ be a rotation matrix such that $\mathbf{R}\bar{\mathbf{x}} = \mathbf{e}_3$. Then the functions $T^r_{\ell,k}(\mathbf{Rz})$, $\forall \mathbf{z} \in \mathcal{C}(\bar{\mathbf{x}}, r)$ are $\mathbb{L}_2(\mathcal{C}(\bar{\mathbf{x}}, r))$-orthonormal, i.e.,

$$\int_{\mathcal{C}(\bar{\mathbf{x}},r)} T^r_{\ell,k}(\mathbf{Rz}) T^r_{\ell',k'}(\mathbf{Rz}) d\omega(\mathbf{z}) = \int_{\mathcal{C}(\mathbf{e}_3,r)} T^r_{\ell,k}(\mathbf{x}) T^r_{\ell',k'}(\mathbf{x}) d\omega(\mathbf{x}) = \delta_{\ell\ell'}\delta_{kk'}.$$

3. Quadrature rules on spherical caps. In this section, we show that spherical cap t-subdesigns induced by a spherical t-design provides equal weight quadrature rules for the numerical integration of zonal polynomials and orthonormal functions $\{T^r_{\ell,k}\}$ over a spherical cap $\mathcal{C}(\mathbf{e}_3, r)$ with radius $r \in (0, \pi)$ and nonnegative weights rules for the numerical integration of spherical harmonics over $\mathcal{C}(\mathbf{e}_3, r)$.

3.1. Quadrature rules for $p \in \mathbb{P}_t(\mathcal{C}(\mathbf{e}_3, r))$. In this subsection, we present positive weights quadrature rules on $\mathcal{C}(\mathbf{e}_3, r)$ by the spherical cap t-subdesign. We begin with the following lemma.

LEMMA 3.1. *Let $\mathcal{C}(\mathbf{e}_3, r)$ be the spherical cap with radius $r \in (0, \pi)$ and $\mathcal{X}_n^{\mathcal{Y}}$ be a spherical cap t-subdesign over $\mathcal{C}(\mathbf{e}_3, r)$ induced by a spherical t-design $\mathcal{Y}_n$. Then, the following quadrature rule is exact for all $T^r_{\ell,k}$ with $\ell \leq t$, $\forall k \in \{1, 2, \ldots, 2\ell + 1\}$,*

$$\frac{1}{2\pi(1 - \cos r)} \int_{\mathcal{C}(\mathbf{e}_3,r)} T^r_{\ell,k}(\mathbf{x}) d\omega(\mathbf{x}) = \frac{1}{n} \sum_{j=1}^{n} T^r_{\ell,k}(\mathbf{x}_j), \ \ \mathbf{x}_j \in \mathcal{X}_n^{\mathcal{Y}}. \tag{3.1}$$

Proof. Let $\kappa = 2/(1 - \cos r)$. For $\ell = 0, 1, \ldots, t$, $k = 1, 2, \ldots, 2\ell + 1$, we have

$$\sum_{j=1}^{n} T^r_{\ell,k}(\mathbf{x}_j) = \sqrt{\kappa} \sum_{j=1}^{n} Y_{\ell,k}(\mathbf{y}_j) = \frac{\sqrt{\kappa} n}{4\pi} \int_{\mathbb{S}^2} Y_{\ell,k}(\mathbf{y}) d\omega(\mathbf{y}) = \begin{cases} \frac{\sqrt{\kappa} n}{\sqrt{4\pi}} & \text{if } \ell = 0 \\ 0 & \text{if } \ell \neq 0, \end{cases}$$

where $\mathbf{y}_j \in \mathcal{Y}_n$, the first equality follows from (2.6), the second equality follows from definition of spherical t-design and the last equality follows from $Y_{0,1}(\mathbf{y}) = 1/\sqrt{4\pi}$, $\forall \mathbf{y} \in \mathbb{S}^2$ and orthogonality of $Y_{\ell,k}$.

On the other hand,

$$\int_{\mathcal{C}(\mathbf{e}_3,r)} T^r_{\ell,k}(\mathbf{x}) d\omega(\mathbf{x}) = \sqrt{\tfrac{4\pi}{\kappa}} \int_{\mathcal{C}(\mathbf{e}_3,r)} T^r_{\ell,k}(\mathbf{x}) T^r_{0,1}(\mathbf{x}) d\omega(\mathbf{x}) = \begin{cases} \sqrt{\frac{4\pi}{\kappa}} & \text{if } \ell = 0 \\ 0 & \text{if } \ell \neq 0, \end{cases}$$

where the second equality follows from $T^r_{0,1}(\mathbf{x}) = \sqrt{\frac{\kappa}{4\pi}}$, $\forall \mathbf{x} \in \mathcal{C}(\mathbf{e}_3, r)$ and the last equality follows from (2.5). The proof is completed. ∎

Based on Lemma 3.1 and Proposition 2.6, we can derive the following nonnegative weights quadrature rule for the numerical integration of spherical harmonics over $\mathcal{C}(\mathbf{e}_3, r)$.

THEOREM 3.2. *Adopts the conditions of Lemma 3.1. Then we have the following equality for any spherical harmonic $Y_{\ell,k}$ of degree at most t,*

(3.2)
$$\int_{\mathcal{C}(\mathbf{e}_3,r)} Y_{\ell,k}(\mathbf{x}) d\omega(\mathbf{x}) = \begin{cases} \frac{2\pi(1-\cos r)}{n} \sum_{j=1}^n Y_{\ell,1}(\mathbf{x}_j) & \text{if } k=1 \\ 0 & \text{otherwise,} \end{cases} \quad \text{where } \mathbf{x}_j \in \mathcal{X}_n^{\mathcal{Y}}.$$

Proof. Since $\int_0^{2\pi} \cos(k\phi) d\phi = 0$ and $\int_0^{2\pi} \sin(k\phi) d\phi = 0$ for any integer k, we have $\int_{\mathcal{C}(\mathbf{e}_3,r)} Y_{\ell,k}(\mathbf{x}) d\omega(\mathbf{x}) = 0$ if $k \neq 1$. By Proposition 2.6, we have

$$\begin{aligned}
\int_{\mathcal{C}(\mathbf{e}_3,r)} Y_{\ell,1}(\mathbf{x}) d\omega(\mathbf{x}) &= \int_{\mathcal{C}(\mathbf{e}_3,r)} \sum_{i=0}^{\ell} \beta_i T^r_{i,1}(\mathbf{x}) d\omega(\mathbf{x}) \\
&= \frac{2\pi(1-\cos r)}{n} \sum_{j=1}^n \sum_{i=0}^{\ell} \beta_i T^r_{i,1}(\mathbf{x}_j) = \frac{2\pi(1-\cos r)}{n} \sum_{j=1}^n Y_{\ell,1}(\mathbf{x}_j),
\end{aligned}$$

where the first and last equalities follow from Proposition 2.6 by taking $k = 1$, and the second equality follows from Lemma 3.1. Thus, we obtain (3.2). ∎

COROLLARY 3.3. *Let $\mathcal{C}(\mathbf{e}_3, r)$ be the spherical cap with radius $r \in (0, \pi)$ and $\mathcal{X}_n^{\mathcal{Y}}$ be a spherical cap $2t$-subdesign over $\mathcal{C}(\mathbf{e}_3, r)$ induced by a spherical $2t$-design $\mathcal{Y}_n$. For any spherical polynomial $p \in \mathbb{P}_t(\mathbb{S}^2)$ of degree $L \leq t$, we have*

$$\int_{\mathcal{C}(\mathbf{e}_3,r)} p(\mathbf{x}) d\omega(\mathbf{x}) = \frac{2\pi(1-\cos r)}{n} \sum_{j=1}^n \sum_{\ell=0}^{L} \alpha_{\ell,1} Y_{\ell,1}(\mathbf{x}_j), \quad \mathbf{x}_j \in \mathcal{X}_n^{\mathcal{Y}}, \tag{3.3}$$

where $\alpha_{\ell,1} = \frac{4\pi}{n} \sum_{j=1}^n p(\mathbf{y}_j) Y_{\ell,1}(\mathbf{y}_j)$, $\mathbf{y}_j \in \mathcal{Y}_n$, $\ell = 0, 1, \ldots, L$.

Proof. For any spherical polynomial $p \in \mathbb{P}_t(\mathbb{S}^2)$ of degree $L \leq t$, there are unique $\alpha_{\ell,k} \in \mathbb{R}$ such that $p = \sum_{\ell=0}^{L} \sum_{k=1}^{2\ell+1} \alpha_{\ell,k} Y_{\ell,k} \in \mathbb{P}_t(\mathbb{S}^2)$. Since $\mathcal{Y}_n$ is a spherical $2t$-design, we have $\alpha_{\ell,k} = \int_{\mathbb{S}^2} p(\mathbf{y}) Y_{\ell,k}(\mathbf{y}) d\omega(\mathbf{y}) = \frac{4\pi}{n} \sum_{j=1}^n p(\mathbf{y}_j) Y_{\ell,k}(\mathbf{y}_j)$, $\ell = 0, 1, \ldots, L \leq t$, $k = 1, 2, \ldots, 2\ell+1$. Moreover,

$$\begin{aligned}
\int_{\mathcal{C}(\mathbf{e}_3,r)} p(\mathbf{x}) d\omega(\mathbf{x}) &= \sum_{\ell=0}^{t} \sum_{k=1}^{2\ell+1} \alpha_{\ell,k} \int_{\mathcal{C}(\mathbf{e}_3,r)} Y_{\ell,k}(\mathbf{x}) d\omega(\mathbf{x}) \\
&= \sum_{\ell=0}^{t} \alpha_{\ell,1} \int_{\mathcal{C}(\mathbf{e}_3,r)} Y_{\ell,1}(\mathbf{x}) d\omega(\mathbf{x}) = \frac{2\pi(1-\cos r)}{n} \sum_{\ell=0}^{t} \sum_{j=1}^{n} \alpha_{\ell,1} Y_{\ell,1}(\mathbf{x}_j),
\end{aligned}$$

where the second equality follows from $\int_{\mathcal{C}(\mathbf{e}_3,r)} Y_{\ell,k}(\mathbf{x}) d\omega(\mathbf{x}) = 0$ if $k \neq 1$, and the third equality follows from Theorem 3.2. The proof is completed. ∎

3.2. Equal weight quadrature rules. In this section, we show that the spherical cap t-subdesign induced by a spherical t-design provides an equal weight quadrature rule that integrates exactly zonal spherical polynomials of degree $\leq t$.

Recall $p = \sum_{\ell=0}^{t} \alpha_{\ell,1} Y_{\ell,1} \in \mathbb{P}_t(\mathcal{C}(\mathbf{e}_3, r))$, where $\alpha_{\ell,1} \in \mathbb{R}$, a zonal polynomial of degree at most t on $\mathcal{C}(\mathbf{e}_3, r)$.

Theorem 3.4. *Let $\mathcal{C}(\mathbf{e}_3, r)$ be the spherical cap with radius $r \in (0, \pi)$ and $\mathcal{X}_n^{\mathcal{Y}}$ be a spherical cap t-subdesign over $\mathcal{C}(\mathbf{e}_3, r)$ induced by a spherical t-design $\mathcal{Y}_n$. Then the following equal weight quadrature*

$$\frac{1}{2\pi(1-\cos r)} \int_{\mathcal{C}(\mathbf{e}_3,r)} p(\mathbf{x}) d\omega(\mathbf{x}) = \frac{1}{n} \sum_{j=1}^{n} p(\mathbf{x}_j), \quad \mathbf{x}_j \in \mathcal{X}_n^{\mathcal{Y}}$$

holds for any zonal polynomial $p \in \mathbb{P}_t(\mathcal{C}(\mathbf{e}_3, r))$ of degree at most t.

Since Theorem 3.4 is a direct result of Theorem 3.2, we omit its proof here.

Next, we present equal weight quadrature rules for the numerical integration of zonal spherical polynomials over any spherical caps with radius $r \in (0, \pi)$.

Lemma 3.5. *Adopt conditions of Theorem 3.4. Let G_L be defined as (2.3), for any $L \le t$, we have*

$$\frac{1}{2\pi(1-\cos r)} \int_{\mathcal{C}(\mathbf{e}_3,r)} G_L(\mathbf{x}, \mathbf{e}_3) d\omega(\mathbf{x}) = \frac{1}{n} \sum_{j=1}^{n} G_L(\mathbf{x}_j, \mathbf{e}_3), \quad \mathbf{x}_j \in \mathcal{X}_n^{\mathcal{Y}}.$$

Proof. Taking $\mathbf{y} = \mathbf{x} \in \mathcal{C}(\mathbf{e}_3, r)$ and $\mathbf{z} = \mathbf{e}_3$ in (2.3), we have

$$G_L(\mathbf{x}, \mathbf{e}_3) = \sum_{\ell=0}^{L} \tfrac{2\ell+1}{4\pi} P_\ell(\mathbf{x} \cdot \mathbf{e}_3) = \sum_{\ell=0}^{L} c_\ell Y_{\ell,1}(\mathbf{x}) \in \mathbb{P}_t(\mathbb{S}^2),$$

where $c_\ell = \frac{2\ell+1}{4\pi N_{\ell,0}}$, $\ell = 0, 1, \ldots, L \le t$. By Theorem 3.4, we obtain this lemma. ∎

Theorem 3.6. *Adopt conditions of Theorem 3.4. Then, for any fixed $\mathbf{z} \in \mathbb{S}^2$ and $L \le t$, we have*

$$\frac{1}{2\pi(1-\cos r)} \int_{\mathcal{C}(\mathbf{z},r)} G_L(\mathbf{y}, \mathbf{z}) d\omega(\mathbf{y}) = \frac{1}{n} \sum_{j=1}^{n} G_L(\mathbf{x}_j, \mathbf{e}_3), \quad \mathbf{x}_j \in \mathcal{X}_n^{\mathcal{Y}}.$$

Proof. For a fixed point $\mathbf{z} \in \mathbb{S}^2$, let $\mathbf{R} \in \mathrm{SO}(3)$ be the rotation matrix of $\mathbf{z}$ such that $\mathbf{R}\mathbf{z} = \mathbf{e}_3$ and $\mathbf{R}\mathbf{y} \in \mathcal{C}(\mathbf{e}_3, r)$ for $\mathbf{y} \in \mathcal{C}(\mathbf{z}, r)$. By the rotational invariance of G_L, we have $G_L(\mathbf{y}, \mathbf{z}) = G_L(\mathbf{R}\mathbf{y}, \mathbf{e}_3)$, $\mathbf{y} \in \mathbb{S}^2$. Thus, for any $L \le t$,

$$\begin{aligned} \int_{\mathcal{C}(\mathbf{z},r)} G_L(\mathbf{y}, \mathbf{z}) d\omega(\mathbf{y}) &= \int_{\mathcal{C}(\mathbf{z},r)} G_L(\mathbf{R}\mathbf{y}, \mathbf{e}_3) d\omega(\mathbf{y}) = \int_{\mathcal{C}(\mathbf{e}_3,r)} G_L(\mathbf{x}, \mathbf{e}_3) d\omega(\mathbf{x}) \\ &= \tfrac{2\pi(1-\cos r)}{n} \sum_{j=1}^{n} G_L(\mathbf{x}_j, \mathbf{e}_3), \end{aligned}$$

where the second equality follows from $\mathbf{x} = \mathbf{R}\mathbf{y}$, $\mathbf{R}^\top \mathbf{R} = \mathbf{I}$ and $\det(\mathbf{R}) = 1$ and the last equality follows from Lemma 3.5. The proof is completed. ∎

In the following, we give the equal weight quadrature rule for the numerical integration of any function f over $\mathcal{C}(\mathbf{e}_3, r)$ that has the following expansion

$$f(\mathbf{x}) = \sum_{\ell=0}^{L} \sum_{k=1}^{2\ell+1} \alpha_{\ell,k} T_{\ell,k}^r(\mathbf{x}), \quad \mathbf{x} \in \mathcal{C}(\mathbf{e}_3, r), \quad \text{where } \alpha_{\ell,k} \in \mathbb{R}. \tag{3.4}$$

Theorem 3.7. *Adopt conditions of Theorem 3.4. Then the quadrature rule*

$$\frac{1}{2\pi(1-\cos r)} \int_{\mathcal{C}(\mathbf{e}_3,r)} f(\mathbf{x}) d\omega(\mathbf{x}) = \frac{1}{n} \sum_{j=1}^{n} f(\mathbf{x}_j), \quad \mathbf{x}_j \in \mathcal{X}_n^{\mathcal{Y}}, \tag{3.5}$$

holds for any function f with expansion (3.4) and $L \le t$.

Proof. By (3.4) and Lemma 3.1, we obtain

$$\begin{aligned}\int_{\mathcal{C}(\mathbf{e}_3,r)} f(\mathbf{x})d\omega(\mathbf{x}) =& \sum_{\ell=0}^{L}\sum_{k=1}^{2\ell+1}\alpha_{\ell,k}\int_{\mathcal{C}(\mathbf{e}_3,r)} T_{\ell,k}^r(\mathbf{x})d\omega(\mathbf{x})\\ =&\frac{4\pi}{\kappa n}\sum_{\ell=0}^{L}\sum_{k=1}^{2\ell+1}\alpha_{\ell,k}\sum_{j=1}^{n} T_{\ell,k}^r(\mathbf{x}_j) = \frac{4\pi}{\kappa n}\sum_{j=1}^{n} f(\mathbf{x}_j),\ \ \mathbf{x}_j\in\mathcal{X}_n^{\mathcal{Y}}.\end{aligned}$$

where $\kappa := 2/(1-\cos r)$. The proof is completed. ∎

Corollary 3.8. *Let $\mathcal{C}(\mathbf{e}_3, r)$ be the spherical cap with radius $r \in (0, \pi)$ and $\mathcal{X}_n^{\mathcal{Y}}$ be a spherical cap $2t$-subdesign over $\mathcal{C}(\mathbf{e}_3, r)$ induced by a spherical $2t$-design $\mathcal{Y}_n$. Then, for any function f with expansion (3.4) and $L \leq t$, we have*

$$\frac{1}{2\pi(1-\cos r)}\int_{\mathcal{C}(\mathbf{e}_3,r)} f(\mathbf{x})T_{\ell,k}^r(\mathbf{x})d\omega(\mathbf{x}) = \frac{1}{n}\sum_{j=1}^{n} f(\mathbf{x}_j)T_{\ell,k}^r(\mathbf{x}_j), \quad \mathbf{x}_j\in\mathcal{X}_n^{\mathcal{Y}},$$
$$\ell = 0, 1, \ldots, L, \quad k = 1, \ldots, 2\ell+1.$$

Proof. Let $\kappa = 2/(1-\cos r)$. By (3.4), we have

$$\begin{aligned}\sum_{j=1}^{n} f(\mathbf{x}_j)T_{\ell,k}^r(\mathbf{x}_j) =& \sum_{j=1}^{n}\sum_{\ell'=0}^{L}\sum_{k'=1}^{2\ell'+1}\alpha_{\ell',k'}T_{\ell',k'}^r(\mathbf{x}_j)T_{\ell,k}^r(\mathbf{x}_j)\\ =&\kappa\sum_{j=1}^{n}\sum_{\ell'=0}^{L}\sum_{k'=1}^{2\ell'+1}\alpha_{\ell',k'}Y_{\ell',k'}(\mathbf{y}_j)Y_{\ell,k}(\mathbf{y}_j)\\ =&\frac{\kappa n}{4\pi}\sum_{\ell'=0}^{L}\sum_{k'=1}^{2\ell'+1}\alpha_{\ell',k'}\int_{\mathbb{S}^2} Y_{\ell',k'}(\mathbf{y})Y_{\ell,k}(\mathbf{y})d\omega(\mathbf{y}) = \frac{\kappa n}{4\pi}\alpha_{\ell,k}\\ =&\frac{\kappa n}{4\pi}\int_{\mathcal{C}(\mathbf{e}_3,r)} f(\mathbf{x})T_{\ell,k}^r(\mathbf{x})d\omega(\mathbf{x}),\end{aligned}$$

where $\mathbf{y}_j \in \mathcal{Y}_n$, the second equality follows from (2.6), the third equality follows from that $\mathcal{Y}_n$ is a spherical $2t$-design, the fourth equality follows from orthogonality of $Y_{\ell,k}$ and the last equality follows from

$$\alpha_{\ell,k} = \int_{\mathcal{C}(\mathbf{e}_3,r)}\sum_{\ell=0}^{L}\sum_{k=1}^{2\ell+1}\alpha_{\ell,k}T_{\ell,k}^r(\mathbf{x})T_{\ell',k'}^r(\mathbf{x})d\omega(\mathbf{x}) = \int_{\mathcal{C}(\mathbf{e}_3,r)} f(\mathbf{x})T_{\ell',k'}^r(\mathbf{x})d\omega(\mathbf{x}).$$

Thus, we complete the proof. ∎

4. Approximation on spherical caps. In this section, we study approximation and sparse signal recovery using orthonormal functions $\{T_{\ell,k}^r\}$ and spherical cap t-subdesigns over the spherical cap $\mathcal{C}(\mathbf{e}_3, r)$ with radius $r \in (0, \pi)$.

4.1. Non-polynomial approximation. Inspired by hyperinterpolation [31], which is a discretization of the $\mathbb{L}_2(\mathbb{S}^2)$ orthogonal projection of a continuous function f on the sphere onto $\mathbb{P}_L(\mathbb{S}^2)$ by a quadrature rule, we study non-polynomial approximation of a continuous function over $\mathcal{C}(\mathbf{e}_3, r)$ by constructing a non-polynomial function through spherical cap t-subdesigns and orthonormal functions $\{T_{\ell,k}^r\}$.

Let $\mathcal{X}_n^{\mathcal{Y}} \subset \mathcal{C}(\mathbf{e}_3, r)$ be a spherical cap t-subdesign induced by a spherical t-design $\mathcal{Y}_n \subset \mathbb{S}^2$ for $t \geq 2L$, following [31], we define the "discrete inner product" corresponding to the $\mathbb{L}_2$ inner product on $\mathcal{C}(\mathbf{e}_3, r)$ as

$$\langle f, g\rangle_n := \frac{2\pi(1-\cos r)}{n}\sum_{j=1}^{n} f(\mathbf{x}_j)g(\mathbf{x}_j), \quad \mathbf{x}_j\in\mathcal{X}_n^{\mathcal{Y}}, \quad f, g\in\mathbb{C}(\mathcal{C}(\mathbf{e}_3, r)),$$

and the non-polynomial approximation of a continuous function $f \in \mathbb{C}(\mathcal{C}(\mathbf{e}_3, r))$ as

$$\mathcal{T}_L f := \sum_{\ell=0}^{L}\sum_{k=1}^{2\ell+1}\langle f, T_{\ell,k}^r\rangle_n T_{\ell,k}^r. \tag{4.1}$$

Notice that $\mathcal{T}_L f \in \mathbb{L}_2(\mathcal{C}(\mathbf{e}_3, r))$. It is easy to verify that

$$\langle T^r_{\ell,k}, T^r_{\ell',k'} \rangle_{\mathbb{L}_2(\mathcal{C}(\mathbf{e}_3,r))} = \langle T^r_{\ell,k}, T^r_{\ell',k'} \rangle_n = \delta_{\ell\ell'}\delta_{kk'} \tag{4.2}$$

for any ℓ, ℓ' satisfying $\ell + \ell' \leq 2L$, $k = 1, \ldots, 2\ell + 1$, $k' = 1, \ldots, 2\ell' + 1$. Hence if $f \in \mathbb{C}(\mathcal{C}(\mathbf{e}_3, r))$ has the exact expansion (3.4) with $2L \leq t$, then $\mathcal{T}_L f = f$.

The following lemma presents a property of $\mathcal{T}_L$.

LEMMA 4.1. *Let $\mathcal{C}(\mathbf{e}_3, r)$ be the spherical cap with radius $r \in (0, \pi)$ and $\mathcal{X}^{\mathcal{Y}}_n$ be a spherical cap t-subdesign induced by a spherical t-design $\mathcal{Y}_n$ for $t \geq 2L$. Given $f \in \mathbb{C}(\mathcal{C}(\mathbf{e}_3, r))$, let $\mathcal{T}_L f$ be defined by (4.1). We have $\langle \mathcal{T}_L f, \mathcal{T}_L f \rangle_n \leq \langle f, f \rangle_n$.*

Proof. By (4.1),

$$\langle \mathcal{T}_L f, T^r_{\ell,k} \rangle_n = \sum_{\ell'=0}^{L} \sum_{k'=1}^{2\ell'+1} \langle f, T^r_{\ell',k'} \rangle_n \langle T^r_{\ell',k'}, T^r_{\ell,k} \rangle_n = \langle f, T^r_{\ell,k} \rangle_n, \quad \forall \ell \leq L,$$

where the last equality follows from (4.2). We obtain $\langle \mathcal{T}_L f, \mathcal{T}_L f \rangle_n = \langle f, \mathcal{T}_L f \rangle_n$. Thus,

$$\langle f - \mathcal{T}_L f, f - \mathcal{T}_L f \rangle_n = \langle f, f \rangle_n + \langle \mathcal{T}_L f, \mathcal{T}_L f \rangle_n - 2\langle f, \mathcal{T}_L f \rangle_n = \langle f, f \rangle_n - \langle \mathcal{T}_L f, \mathcal{T}_L f \rangle_n,$$

which implies $\langle \mathcal{T}_L f, \mathcal{T}_L f \rangle_n \leq \langle f, f \rangle_n$ due to $\langle f - \mathcal{T}_L f, f - \mathcal{T}_L f \rangle_n \geq 0$. ◻

Based on Lemma 4.1, we derive the $\mathbb{L}_2(\mathcal{C}(\mathbf{e}_3, r))$ approximation error bound.

THEOREM 4.2. *Let $\mathcal{C}(\mathbf{e}_3, r)$ be a spherical cap with radius $r \in (0, \pi)$ and $\mathcal{X}^{\mathcal{Y}}_n$ be a spherical cap t-subdesign induced by a spherical t-design $\mathcal{Y}_n$ for $t \geq 2L$. Given $f \in \mathbb{C}(\mathcal{C}(\mathbf{e}_3, r))$, we have*

$$\|\mathcal{T}_L f\|_{\mathbb{L}_2(\mathcal{C}(\mathbf{e}_3,r))} \leq \sqrt{2\pi(1 - \cos r)}\|f\|_\infty, \tag{4.3}$$

$$\|\mathcal{T}_L f - f\|_{\mathbb{L}_2(\mathcal{C}(\mathbf{e}_3,r))} \leq 2\sqrt{2\pi(1 - \cos r)}E_L(f), \tag{4.4}$$

where $E_L(f) := \inf_{\alpha_{\ell,k} \in \mathbb{R}} \|f - \sum_{\ell=0}^{L} \sum_{k=1}^{2\ell+1} \alpha_{\ell,k} T^r_{\ell,k}\|_\infty$.

Proof. Let $\kappa = 2/(1 - \cos r)$. Inequality (4.3) follows from

$$\|\mathcal{T}_L f\|^2_{\mathbb{L}_2(\mathcal{C}(\mathbf{e}_3,r))} = \langle \mathcal{T}_L f, \mathcal{T}_L f \rangle_n \leq \langle f, f \rangle_n = \tfrac{4\pi}{\kappa n} \sum_{j=1}^{n} (f(\mathbf{x}_j))^2 \leq \tfrac{4\pi}{\kappa} \|f\|^2_\infty, \ \mathbf{x}_j \in \mathcal{X}^{\mathcal{Y}}_n,$$

where the first equality follows from (4.2) and the first inequality follows from Lemma 4.1. Now we prove (4.4). Let $h(\mathbf{x}) = \sum_{\ell=0}^{L} \sum_{k=1}^{2\ell+1} \alpha_{\ell,k} T^r_{\ell,k}(\mathbf{x})$, $\mathbf{x} \in \mathcal{C}(\mathbf{e}_3, r)$, where $\alpha_{\ell,k} \in \mathbb{R}$. We have

$$\begin{aligned} \|\mathcal{T}_L f - f\|_{\mathbb{L}_2(\mathcal{C}(\mathbf{e}_3,r))} &= \|\mathcal{T}_L(f - h) + h - f\|_{\mathbb{L}_2(\mathcal{C}(\mathbf{e}_3,r))} \\ &\leq \|\mathcal{T}_L(f - h)\|_{\mathbb{L}_2(\mathcal{C}(\mathbf{e}_3,r))} + \|h - f\|_{\mathbb{L}_2(\mathcal{C}(\mathbf{e}_3,r))} \\ &\leq \sqrt{\tfrac{4\pi}{\kappa}}\|f - h\|_\infty + \sqrt{\tfrac{4\pi}{\kappa}}\|h - f\|_\infty = 4\sqrt{\tfrac{\pi}{\kappa}}\|f - h\|_\infty. \end{aligned} \tag{4.5}$$

Since (4.5) holds for arbitrary $\alpha_{\ell,k} \in \mathbb{R}$, we choose $\alpha_{\ell,k}$ such that $\|f - h\|_\infty = E_L(f)$. we obtain $\|\mathcal{T}_L f - f\|_{\mathbb{L}_2(\mathcal{C}(\mathbf{e}_3,r))} \leq 2\sqrt{2\pi(1 - \cos r)}E_L(f)$. The proof is completed. ◻

Note that if h in (4.5) is a zonal polynomial of degree L, then $E_L(f)$ is the error of best uniform approximation to f by a polynomial of degree at most L, and the convergence rate of $E_L(f)$ has been widely studied, see for example [4, 13] and references therein.

In the following, we give the $\|\cdot\|_\infty$ approximation error bound on $\mathcal{C}(\mathbf{e}_3, r)$.

THEOREM 4.3. *Adopts the conditions of Theorem 4.2. Given $f \in \mathbb{C}(\mathcal{C}(\mathbf{e}_3, r))$, we have*

$$\|\mathcal{T}_L f\|_\infty \le (L+1)\|f\|_\infty, \tag{4.6}$$
$$\|\mathcal{T}_L f - f\|_\infty \le (L+2)E_L(f), \tag{4.7}$$

where $E_L(f) := \inf_{\alpha_{\ell,k}\in\mathbb{R}} \|f - \sum_{\ell=0}^{L}\sum_{k=1}^{2\ell+1} \alpha_{\ell,k} T_{\ell,k}^r\|_\infty$.

Proof. Let $\kappa = 2/(1-\cos r)$, $\mathbf{z} \in \mathcal{C}(\mathbf{e}_3, r)$ be any fixed point and $\mathbf{R_z} = \mathcal{R}(\theta, \phi)$, where $\mathcal{R}(\cdot,\cdot)$ is defined as (2.12) and $(\theta, \phi) \in [0, r] \times [0, 2\pi]$ is the polar coordinate of $\mathbf{z}$, then $\mathbf{R_z z} \in \mathbb{S}^2$ and

$$\begin{aligned}
&|\mathcal{T}_L f(\mathbf{z})| = |\textstyle\sum_{\ell=0}^{L}\sum_{k=1}^{2\ell+1}(\frac{4\pi}{\kappa n}\sum_{j=1}^{n} f(\mathbf{x}_j)T_{\ell,k}^r(\mathbf{x}_j))T_{\ell,k}^r(\mathbf{z})| \\
&= |\textstyle\sum_{j=1}^{n}\frac{4\pi}{n} f(\mathbf{x}_j)\sum_{\ell=0}^{L}\sum_{k=1}^{2\ell+1} Y_{\ell,k}(\mathbf{y}_j)Y_{\ell,k}(\mathbf{R_z z})| \le \|f\|_\infty \sum_{j=1}^{n}\frac{4\pi}{n}|G_L(\mathbf{y}_j, \mathbf{R_z z})| \\
&\le \|f\|_\infty\sqrt{4\pi}(\textstyle\sum_{j=1}^{n}\frac{4\pi}{n}G_L^2(\mathbf{y}_j, \mathbf{R_z z}))^{\frac{1}{2}} = \|f\|_\infty\sqrt{4\pi}(\int_{\mathbb{S}^2} G_L^2(\mathbf{y}, \mathbf{R_z z})d\omega(\mathbf{y}))^{\frac{1}{2}} \\
&= \|f\|_\infty\sqrt{4\pi}G_L^{1/2}(\mathbf{R_z z}, \mathbf{R_z z}) = (L+1)\|f\|_\infty, \quad \mathbf{x}_j \in \mathcal{X}_n^{\mathcal{Y}},\ \mathbf{y}_j \in \mathcal{Y}_n,
\end{aligned}$$

where the second equality follows from Proposition 2.5, G_L is defined as (2.3), the second inequality follows from Cauchy-Schwarz inequality, the third equality follows from definition of $\mathcal{Y}_n$ and the last two equalities follows from Theorem 5.5.2 in [32]. By the arbitrariness of $\mathbf{z} \in \mathcal{C}(\mathbf{e}_3, r)$, we obtain $\|\mathcal{T}_L f\|_\infty \le (L+1)\|f\|_\infty$.

Following a similar proof of (4.5), combing (4.6), we obtain (4.7). ∎

COROLLARY 4.4. *Adopts the conditions of Theorem 4.2, we have*

$$\left|\frac{2\pi(1-\cos r)}{n}\sum_{j=1}^{n} f(\mathbf{x}_j) - \int_{\mathcal{C}(\mathbf{e}_3,r)} f(\mathbf{x})d\omega(\mathbf{x})\right| \le 4\pi(1-\cos r)E_L(f),\ \mathbf{x}_j \in \mathcal{X}_n^{\mathcal{Y}}.$$

Proof. Let $\kappa = 2/(1-\cos r)$. It is easy to see that

$$\begin{aligned}
&\textstyle\int_{\mathcal{C}(\mathbf{e}_3,r)} \mathcal{T}_L f(\mathbf{x})d\omega(\mathbf{x}) = \sum_{\ell=0}^{L}\sum_{k=1}^{2\ell+1}\langle f, T_{\ell,k}^r\rangle_n \int_{\mathcal{C}(\mathbf{e}_3,r)} T_{\ell,k}^r(\mathbf{x})d\omega(\mathbf{x}) = \sqrt{\frac{4\pi}{\kappa}}\langle f, T_{0,1}^r\rangle_n \\
&\qquad = \textstyle\sqrt{\frac{4\pi}{\kappa}}\frac{4\pi}{\kappa n}\sum_{j=1}^{n} f(\mathbf{x}_j)T_{0,1}^r(\mathbf{x}_j) = \frac{4\pi}{\kappa n}\sum_{j=1}^{n} f(\mathbf{x}_j),\ \mathbf{x}_j \in \mathcal{X}_n^{\mathcal{Y}},
\end{aligned}$$

where the second equality follows from orthogonality of $T_{\ell,k}^r$ and $T_{0,1}^r(\mathbf{x}) = \sqrt{\kappa/(4\pi)}$. Then, we obtain

$$\begin{aligned}
&\left|\textstyle\frac{4\pi}{\kappa n}\sum_{j=1}^{n} f(\mathbf{x}_j) - \int_{\mathcal{C}(\mathbf{e}_3,r)} f(\mathbf{x})d\omega(\mathbf{x})\right| = \left|\int_{\mathcal{C}(\mathbf{e}_3,r)} \mathcal{T}_L f(\mathbf{x}) - f(\mathbf{x})d\omega(\mathbf{x})\right| \\
&\le \sqrt{2\pi(1-\cos r)}\|\mathcal{T}_L f - f\|_{\mathbb{L}_2(\mathcal{C}(\mathbf{e}_3,r))} \le 4\pi(1-\cos r)E_L(f),
\end{aligned}$$

where the first inequality follows from Cauchy–Schwarz inequality and the last inequality follows from Theorem 4.2. The proof is completed. ∎

COROLLARY 4.5. *Let m be an integer and f be an m-times continuously differentiable zonal function with all such derivatives in $\mathbb{C}(\mathcal{C}(\mathbf{e}_3, r))$ such that $f(\mathbf{x}) = g(\mathbf{x}\cdot\mathbf{e}_3)$, $\mathbf{x} \in \mathcal{C}(\mathbf{e}_3, r)$, where $g : [\cos r, 1] \to \mathbb{R}$ is m-times continuously differentiable. Then, $E_L(f) := \inf_{\alpha_{\ell,k}\in\mathbb{R}} \|f - \sum_{\ell=0}^{L}\sum_{k=1}^{2\ell+1}\alpha_{\ell,k}T_{\ell,k}^r\|_\infty \le O(L^{-m})$.*

Proof. We adopt the notations in the proof of Theorem 2.8. Define $T_L^r f(\mathbf{x}) = \int_{\mathcal{C}(\mathbf{e}_3,r)} f(\mathbf{z})V_L(\mathbf{R_x x}\cdot\mathbf{R_z z})d\omega(\mathbf{z})$, $\forall \mathbf{x} \in \mathcal{C}(\mathbf{e}_3, r)$, where $\mathbf{R_x} = \mathcal{R}(\theta_1, \phi_1)$ and $\mathbf{R_z} =$

$\mathcal{R}(\theta_2, \phi_2)$ with (θ_1, ϕ_1), $(\theta_2, \phi_2) \in [0, r] \times [0, 2\pi]$ being the polar coordinates of $\mathbf{x}$, $\mathbf{z} \in \mathcal{C}(\mathbf{e}_3, r)$, respectively, and $V_L(\cdot) = \sum_{\ell=0}^{2L-1} \chi(\frac{\ell}{L}) \frac{2\ell+1}{2\pi(1-\cos r)} P_\ell(\cdot)$, where $\chi : [0, \infty) \to [0, 1]$ is a $\mathbb{C}^\infty$ function such that $\chi(s) = 1$, if $0 \le s \le 1$, $\chi(s) = 0$, if $s \ge 2$, and $0 \le \chi(s) < 1$ for $1 < s < 2$. By (2.5) and (2.11), $T_L^r f$ is a zonal polynomial. Then, by Corollary 4.3 in [4], $E_L(f) \le \|f - T_{\lceil L/2 \rceil}^r f\|_\infty \le O(L^{-m})$. ◻

4.2. Sparse signal recovery on the hemisphere. In this section, we apply spherical cap t-subdesigns and orthonormal functions $\{T_{\ell,k}^r\}$ to sparse signal recovery problems on $\mathcal{C}(\mathbf{e}_3, r)$ with radius $r \in (0, \pi)$, where the observed data $\mathbf{c} \in \mathbb{R}^m$ is related to a discrete signal $\mathbf{v}^* \in \mathbb{R}^n$ located on a grid $\mathcal{X}_n \subset \mathcal{C}(\mathbf{e}_3, r)$ according to

$$\mathbf{c} = \mathbf{A}\mathbf{v}^* + \eta,$$

where $\eta \in \mathbb{R}^m$ represents the noise and $\mathbf{A} \in \mathbb{R}^{m \times n}$ is a system matrix, which can be defined by a class of functions and a set of points on $\mathcal{C}(\mathbf{e}_3, r)$. To recovery the signal $\mathbf{v}^*$ on $\mathcal{C}(\mathbf{e}_3, r)$, we use the optimization problem

$$\min_{\mathbf{v} \in \mathbb{R}^m} \|\mathbf{v}\|_q^q := \sum_{i=1}^n |v_i|^q \qquad \text{s.t. } \|\mathbf{A}\mathbf{v} - \mathbf{c}\|_l \le \sigma, \tag{4.8}$$

where $0 < q < 1$, $\sigma > 0$, $l \ge 1$, and the matrix $\mathbf{A} \in \mathbb{R}^{m \times n}$ with elements $(\mathbf{A})_{\ell^2+k,j} = T_{\ell,k}^r(\mathbf{x}_j)$, $\mathbf{x}_j \in \mathcal{X}_n$, $\ell = 0, 1, \ldots, L$, $k = 1, 2, \ldots, 2\ell+1$, $m = (L+1)^2$.

Notice that if $\mathcal{X}_n$ is a spherical cap t-subdesign with $t \ge 2L$, we have $\mathbf{A}\mathbf{A}^\top = \frac{n}{2\pi(1-\cos r)}\mathbf{I}$, which follows from the optimization framework in [10] with $l = 2$.

In this paper, we mainly consider the case that the noise η comes from some heavy-tailed distributions or contains outliers with $l = 1$. We assume that the feasible set of (4.8) is nonempty and $\|\mathbf{c}\|_1 > \sigma$ so that 0 is not a solution. Notice that model (4.8) has been well studied in [38], hence we make a simple sketch of the main results here and refer the reader to [38] for details. By Theorem 2.1 in [38], any solution of problem (4.8) is on the boundary of the feasible set. It is worth noting that by Theorems 2.2 and 2.3 in [38], without any condition on $\mathbf{A}$, there is a $\bar{q} \in (0, 1)$ such that for any $q \in (0, \bar{q}]$, every optimal solution of (4.8) with $l = 1$ is an optimal solution of the following sparse optimization problem

$$\min_{\mathbf{v} \in \mathbb{R}^m} \|\mathbf{v}\|_0 := \sum_{i=1}^n |v_i|^0 \qquad \text{s.t. } \|\mathbf{A}\mathbf{v} - \mathbf{c}\|_1 \le \sigma. \tag{4.9}$$

Since problem (4.8) is nonconvex and non-Lipschitz continuous, it is hard to find an optimal solution. Thus, we will focus on finding a stationary point of (4.8) (see Definition 3.1 in [38]) by solving a sequence of exact penalty problems of (4.8), i.e.,

$$\min_{\mathbf{v} \in \mathbb{R}^m} \|\mathbf{v}\|_q^q + u(\|\mathbf{A}\mathbf{v} - \mathbf{c}\|_1 - \sigma)_+, \tag{4.10}$$

where $u > 0$ is the penalty parameter and $(\cdot)_+ = \max\{\cdot, 0\}$. The exact penalization results can be found in Appendix C in [38]. Due to the nonsmoothness of both parts in (4.10), we apply the smoothing penalty method in [38] for finding a stationary point of (4.8). For details about the algorithm and convergence analysis, see section 3 in [38].

In Subsection 5.3, we show that $\mathbf{v}^*$ can be efficiently recovered by choosing $\mathcal{X}_n$ to be a spherical cap t-subdesign with $t \ge 2L$ using optimization model (4.8) with $l = 1$ when the noises η follow Student's t-distribution.

5. Numerical simulations. In this section, we present numerical evidence on the quality spherical cap t-subdesigns for numerical integration, non-polynomial approximation and sparse signal recovery.

5.1. Geometry of hemispherical t-subdesigns. In this section, we show the geometrical properties of hemispherical t-subdesigns $\mathcal{X}_n^{\mathcal{Y}}$ induced by spherical t-designs $\mathcal{Y}_n$ with $n=(t+1)^2$ [9]. We denote by

$$h(\mathcal{X}_n^{\mathcal{Y}}) := \sup_{\mathbf{y}\in\mathbb{S}^2_+} \min_{\mathbf{x}_j\in\mathcal{X}_n^{\mathcal{Y}}} \operatorname{dist}(\mathbf{y},\mathbf{x}_j) \quad \text{and} \quad \delta(\mathcal{X}_n^{\mathcal{Y}}) := \min_{i\neq j} \operatorname{dist}(\mathbf{x}_i,\mathbf{x}_j)$$

the local mesh norm of $\mathcal{X}_n^{\mathcal{Y}}$ and the separation distance of $\mathcal{X}_n^{\mathcal{Y}}$ with respect to $\mathbb{S}^2_+$, respectively. We know that if $\mathcal{Y}_n = \{\mathbf{y}_1,\ldots,\mathbf{y}_n\}\subset\mathbb{S}^2$ is a spherical t-design, then the set $\mathbf{R}\mathcal{Y}_n=\{\mathbf{R}\mathbf{y}_1,\ldots,\mathbf{R}\mathbf{y}_n\}\subset\mathbb{S}^2$ is a spherical t-design for any rotation matrix $\mathbf{R}\in\mathrm{SO}(3)$. Moreover, $\delta(\mathcal{Y}_n)=\delta(\mathbf{R}\mathcal{Y}_n)$, for any $\mathbf{R}\in\mathrm{SO}(3)$. Let $\mathcal{X}_n^{\mathcal{Y}}$ and $\mathcal{X}_n^{\mathbf{R}\mathcal{Y}}$ be the hemispherical t-subdesigns induced by a spherical t-design $\mathcal{Y}_n$ and the spherical t-design $\mathbf{R}\mathcal{Y}_n$, respectively. Then, we have

$$\min_{\mathbf{R}\in\mathrm{SO}(3)} \delta(\mathcal{X}_n^{\mathbf{R}\mathcal{Y}}) \le \delta(\mathcal{X}_n^{\mathcal{Y}}) \le \max_{\mathbf{R}\in\mathrm{SO}(3)} \delta(\mathcal{X}_n^{\mathbf{R}\mathcal{Y}}). \tag{5.1}$$

In the following, we show the separation distance for hemispherical t-subdesigns $\mathcal{X}_n^{\mathcal{Y}}$ induced by spherical t-designs $\mathcal{Y}_n$ for $t\le 60$ in Figure 1. We also show the separation distance for hemispherical t-subdesigns $\mathcal{X}_n^{\mathbf{R}\mathcal{Y}}$ induced by spherical t-designs $\mathbf{R}\mathcal{Y}_n$, where $\mathbf{R}\in\mathrm{SO}(3)$ is randomly chosen. The local mesh norm of hemispherical t-subdesigns $\mathcal{X}_n^{\mathcal{Y}}$ estimated by using a set of generalized spiral points [6] over the hemisphere with 500,000 points is shown in Figure 1.

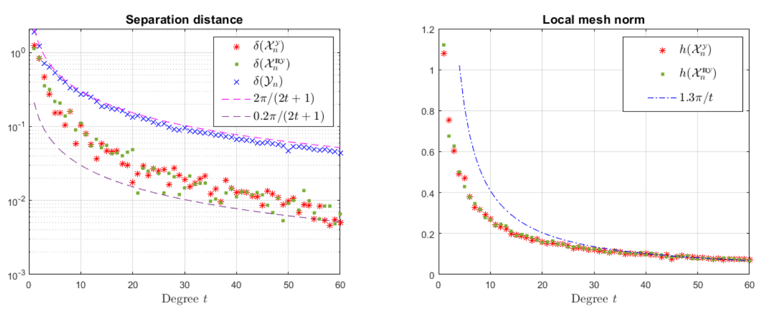

FIG. 1. *Left: the separation distance for hemispherical t-subdesigns and corresponding spherical t-designs with $t=(n+1)^2$. Right: local mesh norm of hemispherical t-subdesigns.*

5.2. Numerical integration and non-polynomial approximation. In this section we apply the hemispherical t-subdesigns $\mathcal{X}_n^{\mathcal{Y}}$ (resp. $\mathcal{X}_n^{\mathbf{R}\mathcal{Y}}$) induced by computed spherical t-designs $\mathcal{Y}_n$ (resp. $\mathbf{R}\mathcal{Y}_n$) with $n=(t+1)^2$ points to evaluate integration and non-polynomial approximation on the hemisphere. We choose the following two functions:

$$\begin{aligned} f_1(\mathbf{x}) =& (4\|\mathbf{x}-\mathbf{e}_3\|+1)((1-\|\mathbf{x}-\mathbf{e}_3\|)_+)^4,\\ f_2(\mathbf{x}) =& ((0.25-\|\mathbf{x}-\bar{\mathbf{x}}\|^2)_+)^3, \end{aligned}$$

where $\mathbf{x}\in\mathbb{S}^2_+$, $\bar{\mathbf{x}}=(1,1,4)/\sqrt{18}$. Note that f_1 is a Wendland function [36] has support $\mathcal{C}(\mathbf{e}_3,\pi/3)$. It is nonsmooth at $\mathbf{e}_3$ and at the boundary of $\mathcal{C}(\mathbf{e}_3,\pi/3)$. f_2 is in the

Solobev space $H^s(\mathbb{S}^2)$ for $s < 3.5$ [22] and has support on a cap $\mathcal{C}(\bar{\mathbf{x}}, \arccos(7/8)) \subset \mathbb{S}^2_+$. It is nonsmooth at the boundary of its support. We also apply spherical cap t-subdesigns $\mathcal{Z}_n^{\mathcal{Y},1}$ and $\mathcal{Z}_n^{\mathcal{Y},2}$ induced by $\mathcal{Y}_n$ to evaluate integration and non-polynomial approximation of f_1 and f_2 on their support sets, i.e., $\Omega_1 := \mathcal{C}(\mathbf{e}_3, \pi/3)$ and $\Omega_2 := \mathcal{C}(\bar{\mathbf{x}}, \arccos(7/8))$, respectively. For convenience, we set $\kappa_1 = 4$ and $\kappa_2 = 16$.

5.2.1. Integration. The approximate values of the integral $\int_{\mathbb{S}^2_+} f_i(\mathbf{x})d\omega(\mathbf{x})$ and $\int_{\Omega_i} f_i(\mathbf{x})d\omega(\mathbf{x})$, $i = 1, 2$, computed by the software Maple are

$$\mathcal{I}_{\mathbb{S}^2_+}(f_1) = \mathcal{I}_{\Omega_1}(f_1) = 0.448798950 \quad \text{and} \quad \mathcal{I}_{\mathbb{S}^2_+}(f_2) = \mathcal{I}_{\Omega_2}(f_2) = 0.003067963.$$

We show the absolute errors $|\mathcal{I}_{\mathbb{S}^2_+}(f_i) - \frac{2\pi}{n}\sum_{j=1}^n f_i(\mathbf{x}_j)|$, $|\mathcal{I}_{\Omega_i}(f_i) - \frac{4\pi}{n\kappa_i}\sum_{j=1}^n f_i(\mathbf{z}_j^i)|$, $\mathbf{x}_j \in \mathcal{X}_n^{\mathcal{Y}}$, $\mathbf{z}_j^i \in \mathcal{Z}_n^{\mathcal{Y},i}$, $i = 1, 2$, as a function of degree t in Figure 2. From Figure 2, we can see that the absolute errors are bounded by $\sqrt{2\pi}\|\mathcal{H}_t f_i(\mathbf{x}) - f_i(\mathbf{x})\|_{\mathbb{L}_2(\mathbb{S}^2_+)}$ $(t \le 30)$, $\sqrt{\pi}\|\mathcal{T}_t f_1(\mathbf{x}) - f_1(\mathbf{x})\|_{\mathbb{L}_2(\Omega_1)}$ $(t \le 30)$, respectively, and decreases rapidly to around 10^{-9} at $t = 60$. Specifically, the absolute error and $\mathbb{L}_2$ error for f_2 are approximately zero for $t \ge 3$. Combing Figure 1, we observe that the separation distance of hemispherical t-subdesigns affect the absolute errors slightly.

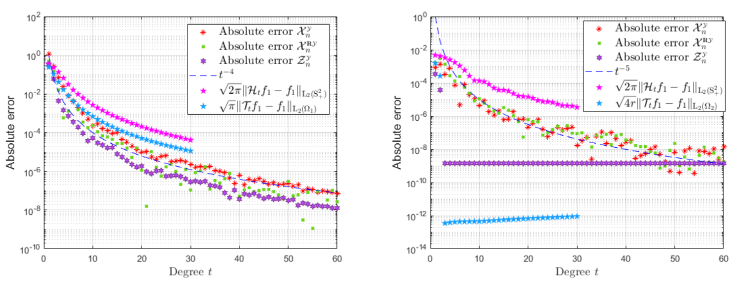

FIG. 2. *Absolute errors for f_1 (left) and f_2 (right).*

5.2.2. Non-polynomial approximation. In this section, we apply hemispherical 60-subdesign $\mathcal{X}_{3721}^{\mathcal{Y}}$ and spherical cap 60-subdesigns $\mathcal{Z}_{3721}^{\mathcal{Y},i}$ induced by a computed spherical 60-design $\mathcal{Y}_{3721}$ to consider the non-polynomial approximation errors for f_i, $i = 1, 2$, on the hemisphere and their support sets, respectively. The $\mathbb{L}_2$ norm of the approximation errors is estimated by

$$\begin{aligned} \|\mathcal{H}_L f_i(\mathbf{x}) - f_i(\mathbf{x})\|_{\mathbb{L}_2(\mathbb{S}^2_+)} &\approx (\tfrac{2\pi}{n}\textstyle\sum_{j=1}^n |f_i(\mathbf{x}_j) - \mathcal{H}_L f_i(\mathbf{x}_j)|^2)^{\frac{1}{2}}, \mathbf{x}_j \in \mathcal{X}_{3721}^{\mathcal{Y}}, \\ \|\mathcal{T}_L f_i(\mathbf{x}) - f_i(\mathbf{x})\|_{\mathbb{L}_2(\Omega_i)} &\approx (\tfrac{4\pi}{n\kappa_i}\textstyle\sum_{j=1}^n |f_i(\mathbf{z}_j^i) - \mathcal{T}_L f_i(\mathbf{z}_j^i)|^2)^{\frac{1}{2}}, \mathbf{z}_j^i \in \mathcal{Z}_{3721}^{\mathcal{Y},i}, \quad i = 1, 2. \end{aligned}$$

The uniform norm of the approximation errors is estimated by

$$\begin{aligned} \|\mathcal{H}_L f_i(\mathbf{x}) - f_i(\mathbf{x})\|_\infty &\approx \max_{\mathbf{x}\in\mathcal{X}^\circ} |f_i(\mathbf{x}) - \mathcal{H}_L f_i(\mathbf{x})|, \\ \|\mathcal{T}_L f_i(\mathbf{z}) - f_i(\mathbf{z})\|_\infty &\approx \max_{\mathbf{z}\in\mathcal{Z}_i^\circ} |f_i(\mathbf{z}) - \mathcal{T}_L f_i(\mathbf{z})|, \quad i = 1, 2, \end{aligned}$$

where $\mathcal{X}^\circ \subset \mathbb{S}^2_+$, $\mathcal{Z}_1^\circ \subset \Omega_1$, $\mathcal{Z}_2^\circ \subset \Omega_2$ are sets of generalized spiral points [6] with 500000, 250000, 62500 points, respectively.

The approximation errors for f_1 and f_2 at every $L \le 30$ are shown in Figures 3 and 4. From Figures 3(a) and 4(a), we observe that the $\mathbb{L}_2$ errors are bounded by uniform errors. In Figures 3(b)-(c) and 4(b)-(c), we show the pointwise errors $|\mathcal{H}_L f_i(\mathbf{x}) - f_i(\mathbf{x})|$ over $\mathcal{X}^\circ$, $|\mathcal{T}_L f_i(\mathbf{z}) - f_i(\mathbf{z})|$ over $\mathcal{Z}_i^\circ$ for $L = 30$, $i = 1, 2$. We observe that the uniform error for f_1 attained at $\mathbf{e}_3$ and the uniform error for f_2 attained at a point around the boundary of spherical cap $\mathcal{C}(\bar{\mathbf{x}}, \arccos(7/8))$. Specifically, the pointwise errors for f_2 estimated on $\mathcal{Z}_2^\circ$ are approximately zero. Besides, the separation distance of hemispherical t-subdesigns does not affect the approximation errors.

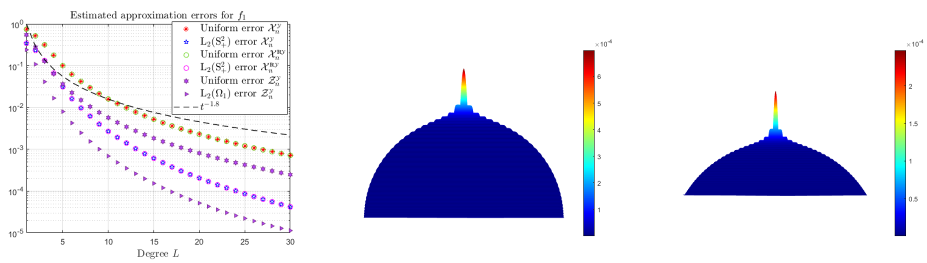

(a) Errors for f_1 (b) Pointwise errors (c) Pointwise errors

FIG. 3. *Estimated approximation errors for f_1.*

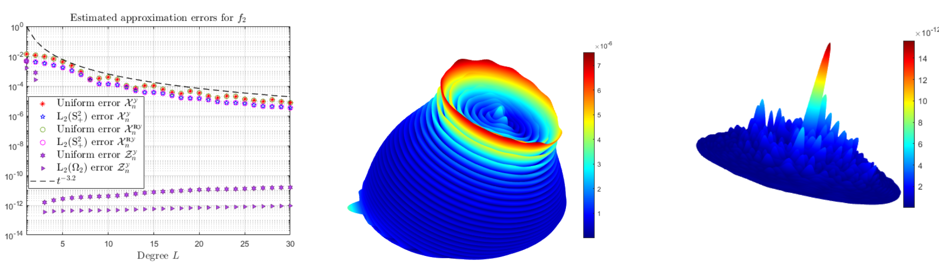

(a) Errors for f_2 (b) Pointwise errors (c) Pointwise errors

FIG. 4. *Estimated approximation errors for f_2.*

We further compare the numerical integration and approximation of f_1 and f_2 over three different domains, i.e., $\mathbb{S}^2$, $\mathbb{S}^2_+$, Ω_1 and Ω_2, using spherical harmonics $\{Y_{\ell,k}\}$ and a spherical t-design $\mathcal{Y}_n$, orthognormal functions $\{H_{\ell,k}\}$ and the hemispherical t-subdesign $\mathcal{X}_n^{\mathcal{Y}}$ induced by $\mathcal{Y}_n$, orthognormal functions $\{T^r_{\ell,k}\}$ and the spherical cap t-subdesign $\mathcal{Z}_n^{\mathcal{Y},i}$ induced by $\mathcal{Y}_n$, $i = 1, 2$, respectively. The results are shown in Figure 5, where the left column is the absolute errors of numerical integration, the middle column is the $\mathbb{L}_2$ approximation errors and the right column is the $\|\cdot\|_\infty$ approximation errors. We observe that the approximation over their support sets achieves the smallest absolute error of numerical integration, $\mathbb{L}_2$ and $\|\cdot\|_\infty$ approximation errors. Thus, both spherical cap t-subdesigns and orthonormal functions $\{T^r_{\ell,k}\}$ are promising for numerical integration and approximation of functions over spherical caps.

5.3. Sparse signal recovery on the hemisphere. To construct the matrix $\mathbf{A}$ and vector $\mathbf{c}$ in optimization problem (4.8), we choose the following four point sets $\mathcal{Y}_n$ on the sphere to derive point sets $\mathcal{X}_n^{\mathcal{Y}}$ on the hemisphere:

- Spherical t-designs (SF).
- Maximum determinant (MD) points [33, 39]: the set of points $\{\mathbf{y}_1, \ldots, \mathbf{y}_n\} \subset \mathbb{S}^2$ which maximizes the determinant of $\mathbf{Y}^\top\mathbf{Y}$, where $(\mathbf{Y})_{\ell^2+k,j} = Y_{\ell,k}(\mathbf{y}_j)$,

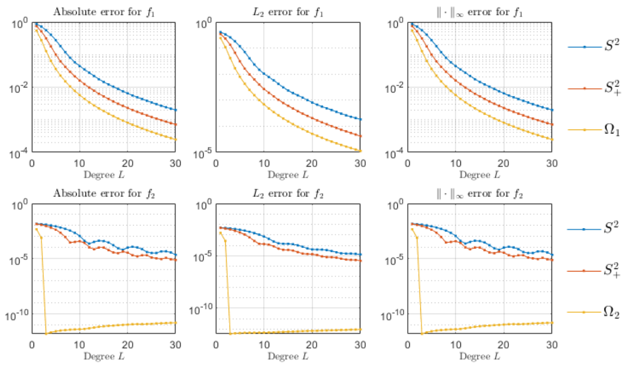

FIG. 5. *Estimated errors of numerical integration (left column), non-polynomial approximation (middle and right columns) for f_1 and f_2.*

$\ell = 0, 1, \ldots, t$, $k = 1, \ldots, 2\ell + 1$, $j = 1, \ldots, n$.

- Tensor product (TP) points: the set of points equally spaced in polar angle $\vartheta \in [0, \pi]$ and azimuthal angle $\phi \in [0, 2\pi)$, i.e., $\vartheta_i = \frac{\pi(2i+1)}{2n_\vartheta}$, $i = 0, 1, \ldots, n_\vartheta - 1$, $\phi_j = \frac{2\pi j}{n_\phi}$, $j = 0, 1, \ldots, n_\phi - 1$, which gives $n = n_\vartheta n_\phi$ distinct points on $\mathbb{S}^2$.
- Gauss-Legendre (GL) points [35]: the set of points uses Gauss-Legendre points with $\cos\vartheta \in (-1, 1)$, $\vartheta \in [0, \pi]$, and equally spaced points in $\phi \in [0, 2\pi)$.

We denote by sSF the hemispherical t-subdesign induced by SF. Similarly, we denote by sMD, sTP and sGL the point sets on $\mathbb{S}^2_+$ induced by MD, TP, GL, respectively in the same way as in Definition 1.1.

The four point sets SF, MD, TP, GL on the sphere were compared in [11] for sparse signal recovery on the sphere. We show some properties of the four point sets sSF, sMD, sTP and sGL on $\mathbb{S}^2_+$ in Table 1, where $\sigma_{\max}(\mathbf{A})$ and $\sigma_{\min}(\mathbf{A})$ are maximal and minimal singular values of $\mathbf{A} \in \mathbb{R}^{(L+1)^2 \times n}$ generated by the four point sets and $\{H_{\ell,k}\}$ with $L = 15$, respectively. In Table 1, the local mesh norm of the four point sets is estimated using spiral points [6] over the hemisphere with 500,000 points. In Figure 6, we show the separation distance $\delta(\mathcal{X}_n^{\mathcal{Y}})$ as a function of the number of points n for sSF, sMD, sGL, and sTP. We show the distribution of points on $\mathbb{S}^2_+$ in Figure 6.

TABLE 1
The four point sets on the hemisphere.

Node	n	t	$h(\mathcal{X}_n^{\mathcal{Y}})$	$\delta(\mathcal{X}_n^{\mathcal{Y}})$	$\delta(\mathcal{X}_n^{\mathcal{Y}})n^{\frac{1}{2}}$	$\sigma_{\max}(\mathbf{A})/\sigma_{\min}(\mathbf{A})$
sSF	1014	44	0.1107	1.8e-2	0.58	1.0000
sMD	1024	31	0.1167	1.6e-2	0.49	1.0605
sTP	1024	30	0.0987	4.8e-3	0.15	3.7733
sGL	1058	45	0.0726	9.9e-3	0.32	3.0508

We apply the smoothing penalty method (SPeL1) proposed in [38] to solve problem (4.8) with $l = 1$, and Algorithm 4.1 in [11] to solve problem (4.8) with $l = 2$.

In the numerical experiments, we first generate $\mathbf{A}$ using sSF, sMD, sGL and sTP as the way in Subsection 4.2 with $L = 15$, respectively. Next we randomly choose a subset $I \subset \{1, 2, \ldots, n\}$ of size $|I|$ with the uniform distribution and generate a vector

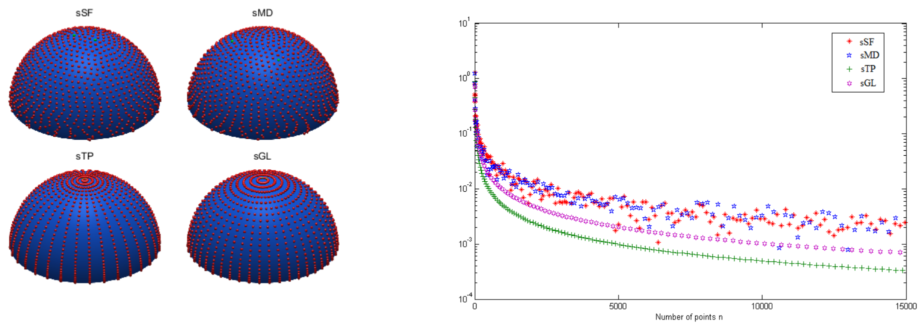

FIG. 6. *The four point sets on the hemisphere (left) and their separation distances (right).*

$\mathbf{u} \in \mathbb{R}^{|I|}$ with i.i.d. standard Gaussian entries. Then, we define the sparse vector $\mathbf{v}^*$ by setting $\mathbf{v}^*_I = \mathbf{u}$ and $\mathbf{v}^*_{I^c} = 0$, and set $\mathbf{c} = \mathbf{A}\mathbf{v}^* + \delta\eta$, where $\delta > 0$ is a scaling parameter and η is the noisy vector with each entry independently following Student's t(2)-distribution. Finally, we set $\sigma = \delta\|\eta\|_l$ for $l = 1, 2$.

The numerical results are presented in Table 2, where $\tilde{\mathbf{v}}$ denotes the recovered signal, "rank" is the rank of $\mathbf{A}_J$ with $J = \mathrm{supp}(\tilde{\mathbf{v}})$, "feasibility" is given by $\max\{\|\mathbf{A}\tilde{\mathbf{v}} - \mathbf{c}\|_l - \sigma, 0\}$ and $\|\mathbf{v}^* \,\&\, \tilde{\mathbf{v}}\|_0$ denotes the number of nonzero elements of $\mathbf{v}^*$ and $\tilde{\mathbf{v}}$ in common and "false" denotes the number of elements that $\mathbf{v}^*$ is zero while $\tilde{\mathbf{v}}$ is nonzero.

TABLE 2
Signal recovery on the hemisphere with different nodes: $\|\mathbf{v}^*\|_0 = |I| = 120$, $q = 0.5$ *and* $\delta = 10^{-3}$.

Nodes	n	feasibility	$\|\mathbf{v}^* - \tilde{\mathbf{v}}\|$	rank	$\|\tilde{\mathbf{v}}\|_0$	$\|\mathbf{v}^* \& \tilde{\mathbf{v}}\|_0$	false
Problem (4.8) with $l = 1$ solved by SPeL1 in [38]							
sSF	1014	0	0.85	133	133	114	6
sMD	1024	0	4.48	200	200	87	33
sGL	1058	0	3.18	129	129	86	34
sTP	1024	0	3.11	115	115	85	35
Problem (4.8) with $l = 2$ solved by Algorithm 4.1 in [11]							
sSF	1014	2.4e-16	2.70	161	161	94	26
sMD	1024	1.0e-16	4.79	196	196	83	37
sGL	1058	0	3.80	144	144	76	44
sTP	1024	0	5.05	137	137	67	53

We also show the recovered signals and pointwise errors by using SPeL1 for problem (4.8) in Figure 7, where the first column illustrates the function values $f(\mathbf{x}_j) = \sum_{\ell=0}^{15}\sum_{k=1}^{2\ell+1} c_{\ell,k} H_{\ell,k}(\mathbf{x}_j)$, $\mathbf{x}_j \in \mathcal{X}_n^{\mathcal{Y}}$ obtained from the noisy coefficients $\mathbf{c}$ and the four point sets. From Table 2 and Figure 7, among the four point sets, the hemispherical t-subdesign (sSF) induced by spherical t-designs performs the best regarding the recovery error and the position of nonzero elements.

6. Conclusion. We first introduce a new set of points on the spherical cap $\mathcal{C}(\mathbf{e}_3, r)$, $r \in (0, \pi)$ and call it the spherical cap t-subdesign induced by the spherical t-design in this paper. Using the relation between spherical harmonics and orthonormal functions $\{T^r_{\ell,k}\}$ established in Section 2, we present an addition theorem for $\{T^r_{\ell,k}\}$ and show that the spherical cap t-subdesign provides an equal weight quadrature rule integrating exactly all zonal polynomials of degree at most t and functions expanded by $\{T^r_{\ell,k}\}$ derived from Legendre polynomials of degree at most t on $\mathcal{C}(\mathbf{e}_3, r)$. Moreover, we apply the spherical cap t-subdesigns and $\{T^r_{\ell,k}\}$ for non-polynomial ap-

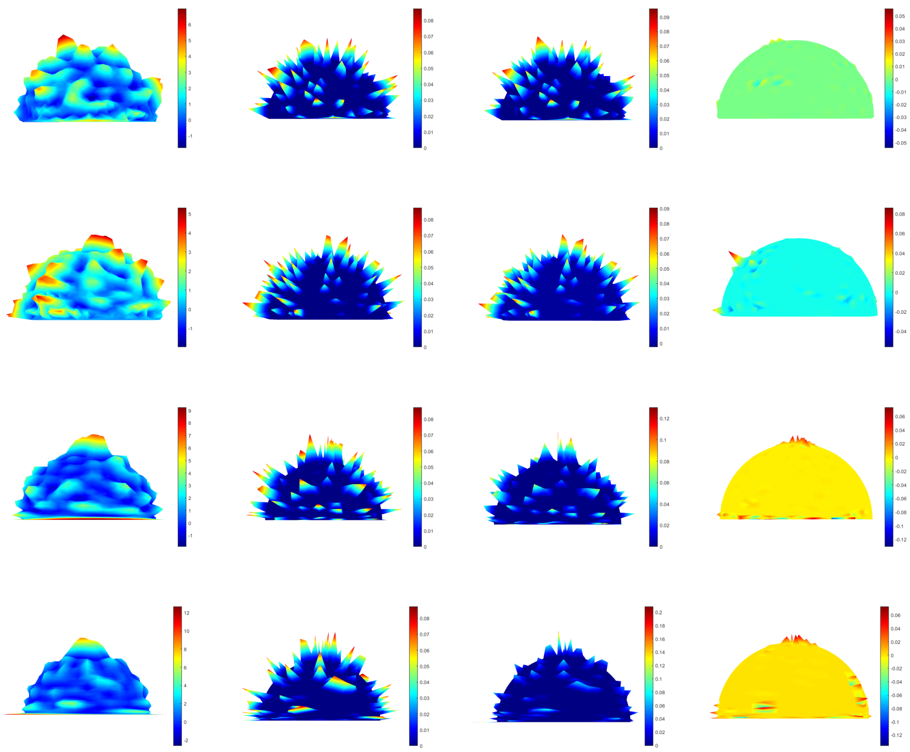

FIG. 7. *Recovery results by the four point sets sSF (row 1), sMD(row 2), sGL(row 3), and sTP(row 4). The function values from noisy coefficients, the true signals, the recovered signals and the pointwise errors are given in column 1 to column 4 at these points, respectively.*

proximation on $\mathcal{C}(\mathbf{e}_3, r)$, and derive error bounds for the approximation. We also apply the spherical cap t-subdesigns to recover sparse signals on $\mathcal{C}(\mathbf{e}_3, r)$. Our theoretical and numerical results show that the spherical cap t-subdesigns are promising for numerical integration and approximation on $\mathcal{C}(\mathbf{e}_3, r)$.

Acknowledgement We would like to thank the Associate Editor and two referees for their very helpful comments.

REFERENCES

[1] C. An, X. Chen, I. Sloan, and R. Womersley, *Well conditioned spherical designs for integration and interpolation on the two-sphere*, SIAM J. Numer. Anal., 48 (2010), pp. 2135–2157.

[2] C. An, X. Chen, I. Sloan, and R. Womersley, *Regularized least squares approximations on the sphere using spherical designs*, SIAM J. Numer. Anal., 50 (2012), pp. 1513–1534.

[3] C. An and H.-N. Wu, *Lasso hyperinterpolation over general regions*, SIAM J. Sci. Comput., 43 (2021), pp. A3967–A3991.

[4] K. Atkinson and W. Han, *Spherical Harmonics and Approximations on the Unit Sphere: An Introduction*, Springer Science & Business Media, 2012.

[5] E. Bannai and E. Bannai, *A survey on spherical designs and algebraic combinatorics on spheres*, Eur. J. Combin., 30 (2009), pp. 1392–1425.

[6] R. Bauer, *Distribution of points on a sphere with application to star catalogs*, J. Guid. Control Dyn., 23 (2000), pp. 130–137.

[7] A. Bondarenko, D. Radchenko, and M. Viazovska, *Optimal asymptotic bounds for spherical designs*, Ann. Math., (2013), pp. 443–452.

[8] J. Brauchart, E. Saff, I. Sloan, and R. Womersley, *QMC designs: optimal order quasi*

monte carlo integration schemes on the sphere, Math. Comput., 83 (2014), pp. 2821–2851.

[9] X. Chen, A. Frommer, and B. Lang, *Computational existence proofs for spherical t-designs*, Numer. Math., 117 (2011), pp. 289–305.

[10] X. Chen and R. S. Womersley, *Existence of solutions to systems of underdetermined equations and spherical designs*, SIAM J. Numer. Anal., 44 (2006), pp. 2326–2341.

[11] X. Chen and R. S. Womersley, *Spherical designs and nonconvex minimization for recovery of sparse signals on the sphere*, SIAM J. Imaging Sci., 11 (2018), pp. 1390–1415.

[12] F. Dai and H. Wang, *Positive cubature formulas and Marcinkiewicz-Zygmund inequalities on spherical caps*, Constr. Approx., 31 (2010), pp. 1–36.

[13] F. Dai and Y. Xu, *Approximation Theory and Harmonic Analysis on Spheres and Balls*, Springer, 2013.

[14] P. Delsarte, J.-M. Goethals, and J. J. Seidel, *Spherical codes and designs*, Geom. Dedicata, 6 (1977), pp. 363–388.

[15] S. Elhabian, H. Rara, and A. Farag, *On the use of hemispherical harmonics for modeling images of objects under unknown distant illumination*, 2011 18th IEEE International Conference on Image Processing, (2011), pp. 1109–1112.

[16] W. Freeden and M. Gutting, *Special Functions of Mathematical (Geo-)Physics*, Springer Science & Business Media, New York, 2013.

[17] P. Funk, *Beiträge zur Theorie der Kugelfunktionen*, Math. Ann., 77 (1915), pp. 136–152.

[18] P. Gautron, J. Křivánek, S. N. Pattanaik, and K. Bouatouch, *A novel hemispherical basis for accurate and efficient rendering*, Rendering Techniques, 2004 (2004), pp. 321–330.

[19] A. Giri, G. P. Choi, and L. Kumar, *Open and closed anatomical surface description via hemispherical area-preserving map*, Signal Process., 180 (2021), p. 107867.

[20] E. Hecke, *Über orthogonal-invariante Integralgleichungen*, Math. Ann., 78 (1917), pp. 398–404.

[21] K. Hesse, I. H. Sloan, and R. S. Womersley, *Local RBF-based penalized least-squares approximation on the sphere with noisy scattered data*, J. Comput. Appl. Math., 382 (2021), p. 113061.

[22] K. Hesse and R. S. Womersley, *Numerical integration with polynomial exactness over a spherical cap*, Adv. Comput. Math., 36 (2012), pp. 451–483.

[23] H. Huang, L. Zhang, D. Samaras, L. Shen, R. Zhang, F. Makedon, and J. Pearlman, *Hemispherical harmonic surface description and applications to medical image analysis*, in Third International Symposium on 3D Data Processing, Visualization, and Transmission (3DPVT'06), IEEE, 2006, pp. 381–388.

[24] S. G. Krantz and H. R. Parks, *A Primer of Real Analytic Functions*, Springer Science & Business Media, 2002.

[25] J. Křivánek, P. Gautron, S. Pattanaik, and K. Bouatouch, *Radiance caching for efficient global illumination computation*, IEEE Trans. Vis. Comput. Graph., 11 (2005), pp. 550–561.

[26] S.-B. Lin, Y. G. Wang, and D.-X. Zhou, *Distributed filtered hyperinterpolation for noisy data on the sphere*, SIAM J. Numer. Anal., 59 (2021), pp. 634–659.

[27] C. Müller, *Analysis of Spherical Symmetries in Euclidean Spaces*, Springer Science & Business Media, New York, 2012.

[28] M. Reimer, *Constructive Theory of Multivariate Functions: with an application to tomography*, BI-Wissenschaftverlag, 1990.

[29] P. D. Seymour and T. Zaslavsky, *Averaging sets: a generalization of mean values and spherical designs*, Adv. Math., 52 (1984), pp. 213–240.

[30] F. J. Simons, F. Dahlen, and M. A. Wieczorek, *Spatiospectral concentration on a sphere*, SIAM review, 48 (2006), pp. 504–536.

[31] I. H. Sloan, *Polynomial interpolation and hyperinterpolation over general regions*, J. Approx. Theory, 83 (1995), pp. 238–254.

[32] I. H. Sloan and R. S. Womersley, *Constructive polynomial approximation on the sphere*, J. Approx. Theory, 103 (2000), pp. 91–118.

[33] I. H. Sloan and R. S. Womersley, *Extremal systems of points and numerical integration on the sphere*, Adv. Comput. Math., 21 (2004), pp. 107–125.

[34] I. H. Sloan and R. S. Womersley, *A variational characterisation of spherical designs*, J. Approx. Theory, 159 (2009), pp. 308–318.

[35] A. H. Stroud, *Approximate Calculation of Multiple Integrals*, Prentice-Hall Series in Automatic Computation, Prentice-Hall, Inc., Englewood Cliffs, N.J., 1971.

[36] H. Wendland, *Scattered Data Approximation*, Cambridge University Press, 2004.

[37] R. S. Womersley, *Efficient spherical designs with good geometric properties*, http://web.maths.unsw.edu.au/ rsw/Sphere/EffSphDes/, (2015).

[38] L. Yang, X. Chen, and S. Xiang, *Sparse solutions of a class of constrained optimization problems*, Math. Oper. Res., 47 (2022), pp. 1932–1956.
[39] Y. Zhou and X. Chen, *Spherical t_ϵ-designs for approximations on the sphere*, Math. Comput., 87 (2018), pp. 2831–2855.

Appendix A. Slepian functions on north polar caps $\mathcal{C}(\mathbf{e}_3, r)$. In this appendix, we give a brief introduction to Slepian functions [30] on $\mathcal{C}(\mathbf{e}_3, r)$ with $r \in (0, \pi]$.

For any $t \in \mathbb{N}_0$, let $d_t := (t+1)^2$ and $\mathbf{D} \in \mathbb{R}^{d_t \times d_t}$ with elements

$$(\mathbf{D})_{\ell^2+k,\ell'^2+k'} = \int_{\mathcal{C}(\mathbf{e}_3,r)} Y_{\ell,k}(\mathbf{x}) Y_{\ell',k'}(\mathbf{x}) d\omega(\mathbf{x}), \tag{A.1}$$

$\ell, \ell' = 0, 1, \ldots, t,\ k = 1, 2, \ldots, 2\ell+1,\ k' = 1, 2, \ldots, 2\ell'+1$. From [30], $\mathbf{D}$ is a real, symmetric and positive definite matrix whose eigenvalues satisfy $1 > \lambda_1 \geq \ldots \geq \lambda_{d_t} > 0$ with corresponding eigenvectors $\mathbf{v}_1, \ldots, \mathbf{v}_{d_t}$. (We choose $\mathbf{v}_1, \ldots, \mathbf{v}_{d_t}$ to be orthonormal.) The Slepian functions [30] are defined by

$$S_i(\mathbf{x}) = \sum_{\ell=0}^{t} \sum_{k=1}^{2\ell+1} v_{\ell,k}^i Y_{\ell,k}(\mathbf{x}),\ i = 1, 2, \ldots, d_t, \quad \forall \mathbf{x} \in \mathbb{S}^2, \tag{A.2}$$

where $\mathbf{v}_i = (v_{0,1}^i, v_{1,1}^i, v_{1,2}^i, v_{1,3}^i, \ldots, v_{t,2t+1}^i)^\top \in \mathbb{R}^{d_t}$ are the eigenvectors of $\mathbf{D}$. The Slepian functions are polynomials of degree $\leq t$ and admit the following property

$$\int_{\mathcal{C}(\mathbf{e}_3,r)} S_i(\mathbf{x}) S_j(\mathbf{x}) d\omega(\mathbf{x}) = \lambda_i \delta_{ij}, \quad \int_{\mathbb{S}^2} S_i(\mathbf{x}) S_j(\mathbf{x}) d\omega(\mathbf{x}) = \delta_{ij}. \tag{A.3}$$

Therefore, for any polynomial $p \in \mathbb{P}_t(\mathbb{S}^2)$, there are unique $\{\alpha_{\ell,k}\}$ and $\{\beta_i\}$ such that

$$p(\mathbf{x}) = \sum_{\ell=0}^{t} \sum_{k=1}^{2\ell+1} \alpha_{\ell,k} Y_{\ell,k}(\mathbf{x}) = \sum_{i=1}^{d_t} \beta_i S_i(\mathbf{x}), \quad \forall \mathbf{x} \in \mathbb{S}^2.$$

Moreover, $\beta_i = \sum_{\ell=0}^{t} \sum_{k=1}^{2\ell+1} \alpha_{\ell,k} v_{\ell,k}^i,\ i = 1, \ldots, d_t$.

It is worth noting that $\int_{\mathcal{C}(\mathbf{e}_3,r)} Y_{\ell,k}(\mathbf{x}) Y_{\ell',k'}(\mathbf{x}) d\omega(\mathbf{x}) = 0$ for $k \neq k'$, thus $\mathbf{D}$ is a sparse matrix. Following our discussions in section 3, let $\mathcal{Z}_{n,r}^{\mathcal{Y}}$ be a spherical cap $4t$-subdesign induced by a spherical $4t$-design $\mathcal{Y}_n$, we obtain

$$(\mathbf{D})_{\ell^2+k,\ell'^2+k} = \tfrac{2\pi(1-\cos r)}{n} \sum_{i=1}^{n} \sum_{\ell''=0}^{\ell+\ell'} c_{\ell'',1} Y_{\ell'',1}(\mathbf{z}_i), \quad \mathbf{z}_i \in \mathcal{Z}_{n,r}^{\mathcal{Y}},$$

where $c_{\ell'',1} = \frac{4\pi}{n} \sum_{j=1}^{n} Y_{\ell,k}(\mathbf{y}_j) Y_{\ell',k}(\mathbf{y}_j) Y_{\ell'',1}(\mathbf{y}_j),\ \mathbf{y}_j \in \mathcal{Y}_n$. Thus, we obtain exact discrete $\mathbf{D}$ on $\mathcal{C}(\mathbf{e}_3, r)$ for any $t \in \mathbb{N}_0$.